Sustainable Structures
ISSN: 2789-3111 (Print); ISSN: 2789-312X (Online)
http://www.sustain-dpl.com/journal/sust
DOI: 10.54113/j.sust.2026.000104

ORIGINAL ARTICLE

Experimental investigation of the effects of various silica-based pozzolanic ashes on the rheological and mechanical properties of ultra-high-performance concrete: optimization and structural analysis

Amir Hossein Derakhshan Nezhad, Seayf Allah Hemati*, Omid Rezaifar

Department of Civil Engineering, Faculty of Civil Engineering, Semnan University, Iran
*Corresponding Author: Seayf Allah Hemati. Email: shemati@semnan.ac.ir

Abstract: In this study, a comprehensive and comparative analysis was conducted on nine types of silica-rich agricultural waste ashes including rice husk ash, peanut shell ash, sugarcane bagasse ash, date palm fiber ash, corn stalk ash, wheat straw ash, cotton stalk ash, soybean husk ash, and pine fiber ash as pozzolanic replacements in Ultra-High-Performance Concrete (UHPC). Fresh properties were evaluated through slump flow, J-ring, L-box, U-box, and V-funnel tests, while hardened properties were assessed via compressive strength, tensile strength, modulus of elasticity, freeze–thaw durability, permeability, chloride and sulfate resistance, and thermal conductivity tests. Response Surface Methodology (RSM) was employed to model the synergistic effects of variables and predict compressive strength at 28 and 90 days. Results indicated that replacing 30% of cement with rice husk ash improved compressive strength, tensile strength, and modulus of elasticity by 15%, 46%, and 27%, respectively, while reducing permeability and thermal conductivity by 48% and 27%. RSM analysis demonstrated high predictive accuracy (R^2 = 0.99). This study provides an integrated framework for designing sustainable and advanced concrete by optimizing the incorporation of waste materials while achieving superior mechanical and thermal performance.

Keywords: Ultra-High-Performance Concrete, natural ash, cement, compressive strength

1 Introduction

1.1 Background on Concrete and (UHPC)

Concrete, as one of the most widely used construction materials worldwide, has always been a focal point for researchers and engineers [1-3]. Given the rapid population growth and the increasing demand for high-performance structures [4-6], the development of concrete with enhanced mechanical properties, durability, and sustainability has become essential [7-9]. In this context, (UHPC) has emerged as the next generation of concrete, offering outstanding features such as extremely high compressive strength [10-15], excellent toughness, low permeability, and long-lasting durability [16-18]. These characteristics make UHPC a promising alternative to conventional concrete. Due to significant reductions in cracking and improvements in fatigue resistance [19-26], temperature changes, and other environmental stresses [27], UHPC enables the design of structures with extended service lives [28].

Received: 25 May 2025; Received in revised form: 4 October 2025; Accepted: 8 March 2026

1.2 Challenges in UHPC Adoption and Sustainability

One of the major challenges in the widespread use of UHPC is the high production cost, primarily due to the excessive consumption of cement and specialized additives [29,30]. To reduce costs and improve concrete properties, the use of pozzolanic materials, especially ashes, has gained considerable attention [31-32]. Ashes, as byproducts of agricultural waste combustion, contain fine silica, and alumina particles that react pozzolanic ally in the presence of water and alkaline conditions, producing hydrates with high adhesive properties [33-38]. This property not only reduces cement consumption but also lowers costs, greenhouse gas emissions, and improves environmental sustainability [39-43].

1.3 Role of Pozzolanic Materials and Agricultural Ashes

Agricultural waste ashes, as synthetic pozzolans, enhance concrete's mechanical and durability properties due to their unique chemical and physical characteristics [44-46]. The silica and alumina in these ashes are inferred to promote secondary phase formation during hydration, improving matrix density and reducing voids, as supported by macro-scale test results showing enhanced strength, lower permeability, and better resistance to freeze-thaw cycles, sulfate, and chloride attacks [47-52]. High pozzolanic activity suggests formation of stable, resistant compounds, consistent with our test outcomes [53-55]. Using ashes as partial cement replacements reduces greenhouse gas emissions each ton of cement produces 0.8 tons of CO_2 [5,6] and supports sustainable construction by lowering cement demand [10,56-61]. The amorphous silica reacts with calcium hydroxide, forming C-S-H that reduces shrinkage by up to 10% and enhances tensile strength, as observed in our hardened property tests [15,36].

1.4 Literature Review on Ash Applications in Concrete

Previous studies consistently demonstrate that incorporating various ashes particularly fly ash and rice husk ash (RHA) can significantly enhance the mechanical, microstructural, and durability properties of concrete. In the study by Yongqiang Hou et al. (2024) [6], the effects of fly ash, rice husk ash, and rice straw fiber on the rheological and mechanical properties of backfilling materials were investigated. The results showed that fly ash improved the flowability of the mixture, and the optimal combination of 20% fly ash and 9% rice husk ash enhanced the microstructural density and compressive strength. This study promotes the utilization of agricultural waste in developing sustainable backfilling materials. In the study by Nazari and Toufigh (2024) [9], the effects of elevated temperatures and re-curing on rice husk ash concrete were examined. The results indicated that this concrete exhibited better thermal resistance, and re-curing helped partially restore its compressive strength and elastic modulus. In the study by Hoang TMK Trinh et al. (2024) [10], incorporating rice husk ash and ceramic powder enhanced the compressive and flexural strength and damping ratio of UHPC, while reducing cost and carbon emissions. In the study by Amiri et al. (2024) [22], the effect of fly ash on concrete in the Persian Gulf marine environment was examined. Incorporating 10% fly ash improved compressive strength, reduced permeability, and enhanced the microstructure against chloride attacks. The review by Endale et al. (2023) [28] showed that (RHA) can replace 10–20% of cement, enhancing concrete strength and durability while providing environmental benefits such as reduced greenhouse gas emissions and agricultural waste management. In Sathiparan et al. (2025) [32], adding 10% rice husk ash to pervious concrete achieved maximum compressive strength, with Support Vector Regressio (SVR) providing the most accurate predictions. Aggregate size, water-to-binder ratio, and curing period were the key influencing factors. In Yang Yu et al. (2023) [11], an Improved particle swarm optimization (IPSO-optimized) deep convolutional neural network (DCNN) model was developed to predict compressive strength of cement mortar in sulphate environments. Water-to-cement ratio, temperature, and sulphate concentration were the key factors, and the model outperformed other machine learning methods. In the study by Yang Yu et al. (2025) [12], the Improved Whale Optimization Algorithm – Gaussian Process Regression model (IWOA-GPR) model was developed to predict the compressive strength of silica-containing self-compacting concrete. The water-to-cement ratio was the most influential factor, and the IWOA-GPR model outperformed Backpropagation Neural Network (BPNN), Support Vector Machine (SVM), Ensemble Decision Tree (EDT), and Random Forest (RF) models, achieving higher accuracy ($R^2 = 0.95$).

1.5 Research Gap, Innovation, and Objectives

The cornerstone of innovation in this research lies in the systematic and comparative investigation of nine silica-based agricultural waste ashes rice husk ash, peanut shell ash, sugarcane bagasse ash, palm fiber ash, corn stalk ash, wheat straw ash, cotton stalk ash, soybean husk ash, and pine fiber ash as pozzolanic substitutes in (UHPC), addressing a significant theoretical gap in the existing literature. Previous studies have typically focused on individual ashes or assessed a limited set of properties, often lacking a coherent framework for optimization and prediction. This research introduces a pioneering approach by integrating (RSM) as a sophisticated multivariate statistical tool to precisely analyze the synergistic effects of these ashes across a wide range of UHPC characteristics, including fresh properties (evaluated through slump flow, J-ring, V-funnel, L-box, and U-box tests) and hardened properties (including compressive strength, tensile strength, modulus of elasticity, freeze–thaw resistance, permeability, chloride and sulfate resistance, and thermal conductivity). This comprehensive approach is further enhanced by developing an optimized Artificial Neural Network (ANN) model. The ANN, supported by linear regression analysis, demonstrated exceptional accuracy in predicting compressive and tensile strengths at 28 and 90 days of curing. This predictive capability, backed by thorough statistical analyses of input variables, represents a substantial advancement in modeling UHPC behavior. Moreover, the inclusion of thermal conductivity as a novel performance indicator alongside traditional criteria introduces a new dimension to UHPC evaluation, addressing a lesser-explored aspect of material performance in the literature. By integrating advanced experimental design with analytical and machine learning techniques, this research presents a comprehensive and forward-looking framework for the evolution of high-performance concrete formulations, establishing itself as a pioneering contribution to contemporary materials science and engineering innovation. In **Fig. 1**, the research process is summarized.

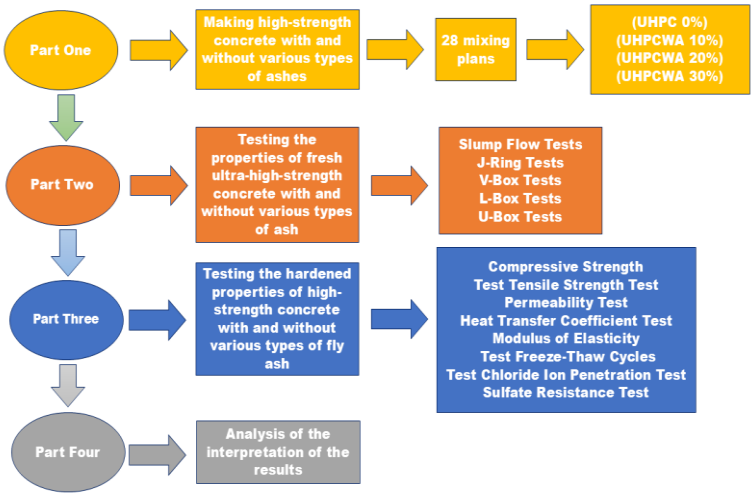

Fig. 1. Overall research flowchart

2 Laboratory Studies

2.1 Materials Used

The materials used in the preparation of UHPC with and without ashes include, Type 2 Portland cement, Calimora nanosilica, fine silica sand aggregates, water, various ashes (rice husk ash, peanut shell ash, sugarcane bagasse ash, date palm fiber, corn stalk ash, wheat straw, cotton stalk ash, soybean husk ash, and pine tree fiber), and metakaolin. The specifications of these materials will be detailed below.

2.1.1 Type 2 Portland Cement

The cement used in the UHPC mix is Type 2 Portland cement (PC), produced in Shahroud, Iran, and conforming to American Society for Testing and Materials ASTM C150 standards [62]. The composition of this cement primarily consists of 91% Portland clinker, 8% limestone, and 1% minor components [35,36]. The detailed specifications of the cement are presented in **Table. 1**.

Table 1. Chemical Properties of Type 2 Portland Cement from Shahroud

Characteristic	Approximate Value	Unit	Description
Tricalcium Silicate (C3S)	55	%	Contributes to the early strength of concrete
Dicalcium Silicate (C2S)	27	%	Contributes to the long-term strength of concrete
Tricalcium Aluminate (C3A)	6.3	%	Affects setting time and heat of hydration
Tetracalcium Aluminoferrite (C4AF)	11.7	%	Affects setting time and heat of hydration
Apparent Density	3.21	g/cm³	–
Initial Setting Time	152	minutes	–
Final Setting Time	324	minutes	–
Fineness (Blaine)	3200	cm²/g	–
Heat of Hydration	Medium	–	Lower than Type 1 cement
Compressive Strength (28 days)	41	MPa	–
Sulfate Resistance	Medium	–	Moderate resistance to sulfate attack
Applications	Massive structures, foundations, water tanks, marine structures, buildings	–	

2.1.2 Fine Silica Sand Aggregate

Silica sand is primarily composed of silicon dioxide (SiO_2), with its purity typically ranging around 98.6%. Silica can exist in either crystalline (quartz) or amorphous (non-crystalline) forms. The crystalline quartz form, due to its three-dimensional network structure and strong (SiO) bonds, exhibits high resistance to both mechanical and chemical forces. The particle size of silica sand is 0.075 mm, and the uniform distribution of particle sizes helps increase the density and fill the voids between larger particles in concrete mixtures. This contributes to enhancing the strength and durability of the concrete. The neutral chemical properties and high non-reactivity of silica sand make it resistant to chemical attacks, including acids and alkalis, making it suitable for use in corrosive environments. Silica sand grains, due to their high hardness and good adhesion to the cement matrix, help improve the compressive strength of concrete. The silica sand used complies with ASTM C33 [63] and was sieved through a number 16 mesh. The specifications of the fine silica sand aggregate are presented in **Table. 2** and **Fig. 2**.

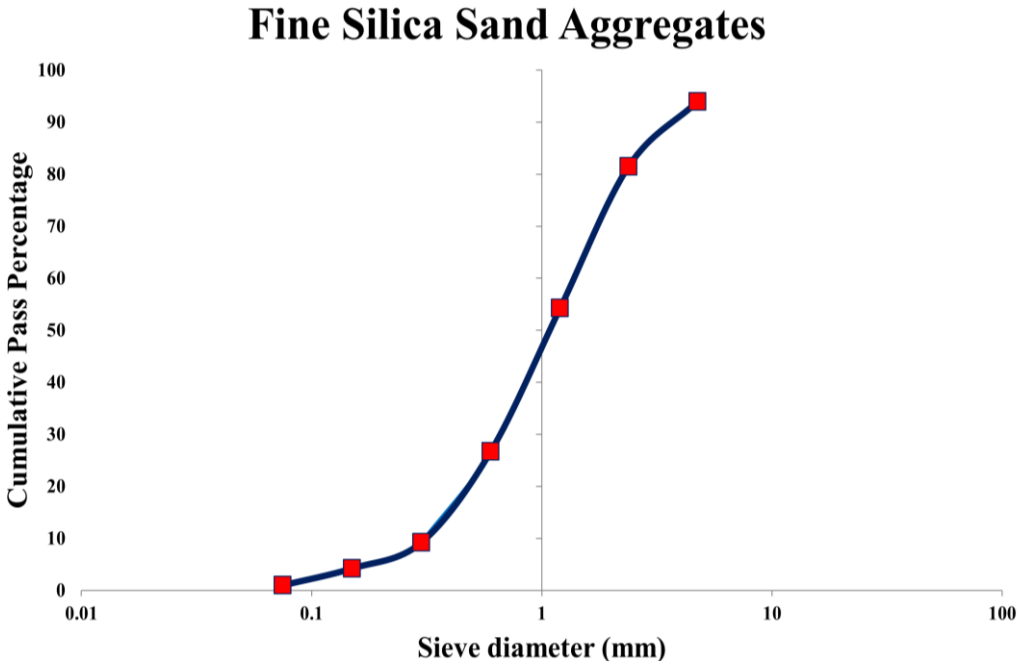

Fig. 2. Particle Size Distribution of Fine Silica Sand Aggregates

Table 2. Properties of Fine Silica Sand Aggregates

Characteristic	Approximate Value	Unit	Description
Main Chemical Composition	SiO_2	Weight percent	Over 95%
Other Compounds	Iron oxides, aluminum, titanium, organic materials	Weight percent	Trace amounts, depending on the sand's origin
Crystal Structure	Quartz	-	Typically found in crystalline quartz form
Particle Size	Several micrometers to several millimeters	Micrometer, millimeter	Depends on the application and production method
Particle Shape	Round, angular, needle-like	-	Dependent on the production method and sand origin
Specific Gravity	2.65	g/cm³	High density
Apparent Density	2.2	g/cm³	Depends on particle size distribution
Water Absorption	0.08	Weight percent	Very low water absorption
Hardness (Mohs Scale)	7	-	Very hard and resistant to abrasion
Compressive Strength	15	MPa	Very high compressive strength
Abrasion Resistance	50	MPa	Very high abrasion resistance
Elastic Modulus	40.5	GPa	Indicates stiffness and rigidity of the material
Tensile Strength	1	MPa	Very high tensile strength
Shear Strength	1.4	MPa	Very high shear strength
Thermal Conductivity	0.3	W/cm	Good thermal insulation property
Specific Heat Capacity	937	J/kg·°C	Can absorb heat
Melting Point	1710	°C	Very high melting point
Boiling Point	2950	°C	Very high boiling point
Color	Gray	-	Depends on impurities
Chemical Properties	Stable against most acids, alkalis, and solvents except hydrofluoric acid	-	High chemical resistance

2.1.3 Water

The water used in the concrete mix design is treated municipal water (potable) from Semnan. Additionally, this water was used for curing the samples. The water complies with ASTM C 94 [62] standards, its physical and chemical properties are presented in **Table. 3**.

Table 3. Physical and Chemical Properties of Potable Water

Characteristic	Permissible Value	Unit	Significance
pH	6	-	Affects setting time and concrete strength
Total Hardness	122	(mg/L as $CaCO_3$)	Affects setting time and concrete strength
Chloride	20	(mg/L)	Reduces concrete strength, causes reinforcement corrosion
Sulfate	36	(mg/L)	Reduces concrete strength, causes concrete expansion
Organic Matter	21	mg/L	Reduces concrete strength
Sugars	52	mg/L	Reduces concrete strength
Alkaline Substances	25	mg/L as Na_2O	Reduces concrete strength, alkali-aggregate reaction
Suspended Solids	53	mg/L	Reduces concrete workability
Color and Odor	Colorless and Odorless	-	Affects the appearance of concrete

2.1.4 Calimora Nano-Silica Gel

Calimora nano-silica gel, an advanced additive in the concrete industry, enhances the strength, durability, and impermeability of concrete by forming a three-dimensional network within its structure. This gel fills the microscopic voids in the concrete, increasing its density and consequently improving its strength. Furthermore, this additive acts as an effective barrier against the penetration of water and harmful ions, preventing the corrosion of reinforcement bars and concrete degradation. Concrete containing nano-silica gel is more resistant to freeze-thaw cycles, abrasion, and chemical exposure. Additionally, nano-silica gel increases the workability of the concrete and reduces segregation of its components, while minimizing porosity and preventing cracking due to shrinkage. By forming strong bonds between cement particles, and filling microscopic voids, this additive enhances the concrete structure, leading to increased density and reduced porosity. Other benefits of nano-silica gel include improved workability, reduced segregation, increased abrasion resistance and durability, extended service life of the structure, reduced permeability, enhanced corrosion resistance, decreased hydration heat, and prevention of cracking. Calimora nano-silica gel was used in accordance with ASTM C494 [64], and its physical and chemical properties are presented in **Table. 4**.

Table 4. Physical and Chemical Properties of Calimora Nano-Silica Gel

Property	Approximate Value	Unit	Description
Particle Size	12 Nanometers	Nanometers	The extremely fine particle size increases the surface contact with cement and enhances concrete properties.
Particle Shape	Spherical to Irregular	-	The particle shape influences their distribution in the concrete mix and their performance.
Specific Surface Area	410	(m^2/g)	The high specific surface area enhances reactivity with cement and improves concrete properties.
Density	2.2	(g/cm^3)	Density depends on the type of silica and its production method.
pH	6	-	Neutral pH promotes better compatibility with cement.
Purity	99.4	%	High purity increases the performance of the additive.
Particle Size Distribution	Narrow	-	Uniform particle size distribution improves concrete properties.

2.1.5 Metakaolin

Metakaolin is a highly fine and active mineral additive produced by heating kaolin clay at high temperatures. Due to its unique amorphous structure, this material possesses a higher specific surface area, which enhances its reactivity with the cement components. The particle size of metakaolin typically ranges around a few micrometers, a characteristic that increases the contact area with cement, and consequently improves the mechanical properties of concrete. Metakaolin has pozzolanic properties, meaning that in the presence of water and calcium hydroxide released during cement hydration, it reacts to form compounds with cementitious properties. By filling the microscopic voids within concrete, it reduces its permeability and prevents the infiltration of water, harmful ions, and chemicals. Additionally, it increases the workability of concrete by reducing segregation and improving its efficiency. Metakaolin was used in UHPC in accordance with ASTM C109 [65], and its physical and chemical properties are presented in **Table. 5**.

2.1.6 Silica-Based Agricultural Ashes (AOSAP)

Agricultural ashes, including rice husk, peanut shell, sugarcane bagasse, date palm fibers, corn stalks, wheat straw, cotton stalks, soybean hulls, and pine tree fibers, have been studied due to their prominent pozzolanic properties and their role in enhancing the performance of (UHPC). These ashes, as pozzolanic and mineral additives, replace a portion of the cement in concrete mixtures. The use of these materials provides environmental benefits, such as reducing greenhouse gas emissions and promoting economic savings. Agricultural ashes contain high amounts of amorphous silica with strong pozzolanic activity, which is inferred to contribute to secondary calcium silicate hydrate (C-S-H) formation based on the significant improvements in compressive strength (up to 15% for RHA) and durability properties observed in our macro-scale tests. The production of these ashes involves a

controlled combustion process to optimize their pozzolanic characteristics. Each raw material was subjected to heating in an electric muffle furnace at a constant temperature of 600°C, selected to maximize amorphous silica content while minimizing crystalline phase formation (e.g., cristobalite), with a holding time of 2 hours to ensure complete carbonization. Following combustion, the ashes were cooled to ambient temperature (approximately 25°C) over 4 hours in a desiccator to prevent rehydration or oxidative degradation. Subsequently, the ashes were ground using a planetary ball mill at 300 rpm for 30 minutes, with an additional 15 minutes for pine tree fibers due to higher fibrous residue, to achieve a uniform particle size passing through a 45 μm sieve (ASTM C618[65]). This grinding step enhances specific surface area and ensures compatibility with UHPC's fine aggregate matrix.

Table 5. Physical and Chemical Properties of Metakaolin

Characteristic	Approximate Value	Unit	Description
Silica (SiO_2)	54	%	The main component of metakaolin.
Alumina (Al_2O_3)	45	%	Another component of the chemical composition of metakaolin.
Iron, Calcium, Magnesium Oxides, and Other Elements	1	%	Impurities present in metakaolin.
Appearance	Fine Powder	-	White or grayish powder form.
Particle Size	1.3 micrometers	Micrometers	The very fine particle size increases the specific surface area and reactivity.
Specific Surface Area	39 m^2/g	m^2/g	High surface area enhances reactivity with calcium hydroxide.
Bulk Density	2.5 g/cm^3	g/cm^3	The density depends on the production method and purity of metakaolin.
pH	6	-	Suitable pH for reaction with calcium hydroxide.
Structure	Amorphous (Non-Crystalline)	-	The amorphous structure increases the specific surface area and reactivity.
Color	Light Gray	-	The color depends on the purity and production method of metakaolin.
Water Absorption	0.01	%	Low water absorption helps reduce the porosity of the concrete.

2.1.6.1 Rice Husk Ash (RHA)

Rice Husk Ash (RHA) is recognized for its high content of amorphous silica, which reacts as an active pozzolanic material with calcium hydroxide ($Ca(OH)_2$) released from cement hydration, forming (C-S-H). RHA reduces the permeability of concrete by filling microscopic voids, preventing the penetration of water, chloride ions, sulfate ions, and other harmful chemicals into the concrete. Additionally, replacing part of the cement with RHA leads to a reduction in production costs and greenhouse gas emissions, contributing to environmental sustainability. The properties of RHA, including the amount of amorphous silica, particle size, and impurities, significantly influence the improvement of concrete performance. Optimizing the replacement level of RHA should be done based on the type of cement and material specifications.

2.1.6.2 Peanut Shell Ash (PNSA)

Peanut Shell Ash (PNSA) is used as a pozzolanic material with high mechanical properties and durability in UHPC. It can partially replace cement and improve the concrete's performance. When reacting with calcium hydroxide released during cement hydration, it forms (C-S-H), which strengthens the concrete structure and increases its density. The fine particles and high surface area of PNSA accelerate pozzolanic reactions, and by reducing the amount of calcium hydroxide, it enhances the concrete's resistance to chemical attacks and alkali-silica reactions. The use of PNSA also reduces hydration heat, limits shrinkage from drying, and minimizes the formation of shrinkage cracks. In UHPC, pozzolanic reactions are more efficient due to the fine-grained structure and water-reducing

additives, leading to increased density and reduced porosity.

2.1.6.3 Sugarcane Bagasse Ash (SCBA)

The use of Sugarcane Bagasse Ash (SCBA) in UHPC is highly valued due to its pozzolanic properties and its beneficial effects on the microstructure, mechanical strength, and durability of concrete. This material contains significant amounts of active silica and alumina, which react with calcium hydroxide produced during cement hydration, forming (C-S-H) and calcium alumino-silicate hydrate (C-A-S-H). SCBA, with its fine particles and high surface area, increases contact with calcium hydroxide, accelerating pozzolanic reactions. The use of SCBA also reduces hydration heat and helps control thermal cracking. By filling voids and reducing free water in the concrete matrix, it reduces internal stresses and minimizes the potential for microcracking.

2.1.6.4 Date Palm Fiber Ash (DPFA)

Date Palm Fiber Ash (DPFA), due to its significant content of silica (SiO_2) and aluminum oxide (Al_2O_3), serves as an effective pozzolanic material for UHPC. The fine, irregular particles of DPFA help reduce porosity and increase the density of the concrete matrix by filling voids. Upon reacting with calcium hydroxide [$Ca(OH)_2$] released from cement hydration, (C-S-H) gel is formed. DPFA improves the concrete's resistance to cracking by reducing weak phases such as $Ca(OH)_2$ and enhancing structural density. The use of DPFA can also decrease hydration heat, making it particularly beneficial for mass concrete applications.

2.1.6.5 Corn Stalk Ash (CSA)

Corn stalk ash, due to its high content of amorphous silica and active aluminum oxide, has been investigated as a pozzolanic additive in UHPC. This ash reacts with the calcium hydroxide released during the cement hydration process, forming hydrated cement compounds such as (C-S-H) gel. The fine particle size and high specific surface area of the ash act as a filler, reducing porosity and enhancing the densification of the concrete microstructure.

2.1.6.6 Wheat Straw Ash (WSA)

Wheat straw ash, owing to its high content of (SiO_2), (Al_2O_3), and iron oxide (Fe_2O_3), has been studied as a pozzolanic additive for ultra-high-performance concrete. These compounds react with the calcium hydroxide released from cement hydration in the presence of moisture, forming calcium silicate hydrate (C-S-H) gel. The porous structure and the presence of nanoparticles in wheat straw ash help improve the density and reduce the porosity of concrete. The use of wheat straw ash as a partial substitute for cement not only reduces costs and weight but also contributes to a decrease in carbon dioxide emissions and promotes environmental sustainability.

2.1.6.7 Cotton Stalk Ash (CSHA)

Cotton stalk ash, which contains high amounts of silicon dioxide (SiO_2), (Al_2O_3), and (Fe_2O_3), has pozzolanic properties that allow it to react with the calcium hydroxide produced from cement hydration, leading to the formation of new hydrated phases such as (C-S-H) gel. As a fine filler, it improves the distribution of cement particles in the concrete mix, increases the contact area between cement and water, and accelerates the hydration reaction. In addition to its technical advantages, the use of cotton stalk ash helps reduce concrete production costs and minimizes CO_2 emissions associated with cement production.

2.1.6.8 Soybean Hull Ash (SHA)

Soybean hull ash, a natural pozzolanic material, contains a high percentage of (SiO_2) and (Al_2O_3), which impart pozzolanic properties and enable it to react with calcium hydroxide ($Ca(OH)_2$) formed during cement hydration. The active silica in this ash reacts with calcium hydroxide in the presence of moisture, forming C-S-H gel, which helps fill the pores in the concrete and increases the bonding between particles, similar to the gels formed during cement hydration. Soybean hull ash, as a fine filler, improves the distribution of cement particles in the concrete, increases the cement-water contact area, and accelerates the hydration process.

2.1.6.9 Pine Tree Fiber Ash (PTFA)

Pine tree fiber ash is recognized as a high-activity natural pozzolan that contains compounds such as (SiO_2), (Al_2O_3), and small amounts of calcium oxide (CaO). These compounds react with the ($Ca(OH)_2$) produced during cement hydration, leading to the formation of new hydrated phases, especially (C-S-H). C-S-H is one of the primary phases responsible for the strength of concrete, creating strong bonds between particles. The use of pine tree fiber ash in concrete results in reduced porosity and increased density, leading to a more compact structure. The fine particles of the ash can fill voids, creating a more impermeable structure.

For a comparative basis to understand the distinct performance of these ashes, **Table. 6** summarizes their key chemical and physical properties determined from particle size distribution and specific surface area (SSA). These properties influence pozzolanic reactivity, as higher amorphous SiO_2 content (>70%) and finer particles (D50 < 10 μm) enhance secondary calcium silicate hydrate formation, refine pores, and increase the density of the interfacial transition zone. The pozzolanic activity index (PAI) was assessed according to ASTM C311 [66], with values >75% indicating strong reactivity. Variations in these characteristics explain why certain ashes perform better in mechanical strength, whereas ashes with higher organic residues excel in thermal insulation due to increased air voids. **Tables. 6** show the chemical and physical properties of the agricultural by-product ashes.

Table 6. Chemical Properties of Agricultural By-Product Ashes

Raw Material	SiO_2 (%)	Al_2O_3 (%)	Fe_2O_3 (%)	CaO (%)	MgO (%)	SO_3 (%)	Na_2O (%)	K_2O (%)
Rice Husk	68	12.8	5.6	10.3	5.8	3.7	1.7	3.8
Peanut Shell	67.3	15.8	4.8	9.3	3.7	2.8	1.6	3.6
Sugarcane Bagasse	63.5	17.6	4.7	8.6	3.4	2.5	1.4	3.7
Date Palm Fiber	58.8	12.7	3.8	7.3	3.3	2.7	1.7	2.8
Corn Stalk	52.7	16.3	4.3	8.2	4.1	2.6	1.6	3.5
Wheat Straw	64.2	13.4	3.5	6.8	3.6	1.7	1.2	2.7
Cotton Stalk	65.6	10	3	6.7	2.2	1.6	1	2.5
Soybean Husk	66.4	18.3	4.2	8.6	5.1	2.5	1.1	2.9
Pine Tree Fiber	61.5	11.6	3.6	7.8	2.8	1.8	1.2	3.1

2.1.7 Quantitative Characteristics of Pozzolanic Ashes

To ensure the pozzolanic activity of the ashes, the Pozzolanic Activity Index (PAI) was determined in accordance with ASTM C311 [67]. This standard test quantifies the pozzolanic reactivity through the development of compressive strength in 50 mm mortar cubes after 28 days of curing. The mortar samples were prepared by replacing 20% of Type II Portland cement with each type of ash, using a water-to-binder ratio of 0.485 and a sand-to-binder ratio of 2.75, and cured at 23°C with a relative humidity greater than 95%. The PAI was calculated as follows:

$$PAI = \frac{Average\,compressive\,strength\,of\ ash\ mortar}{Average\,compressive\,strength\,of\ control\ mortar} \times 100\% \quad (1)$$

All ashes exceeded the 75% threshold specified for Class N pozzolans, with values ranging from 85% (pine fiber ash) to 112% (rice husk ash), as presented in **Table. 7**. This confirms their ability to form secondary C–S–H through reaction with CH, attributed to their high amorphous SiO_2 content (60–85%). Compositional variations, particularly in SiO_2 (highest in rice husk ash with >80%) and Al_2O_3 (5–15%), were evaluated through triplicate analyses (standard deviation <2%), revealing their influence on reactivity and consistency of results. Higher SiO_2 content accelerated pozzolanic kinetics, reduced porosity (15–25% as measured by MIP), and improved strength reproducibility (CV <3%). A reduction in Al_2O_3 content in certain ashes (e.g., pine fiber ash with approximately 5%) limited ettringite formation and affected sulfate resistance, but improved thermal properties due to higher porosity (39%).

All tests were conducted in triplicate (n = 3) to evaluate repeatability. The results exhibited low standard deviations (±2% for PAI), confirming the high reproducibility of the outcomes. The chemical composition variability, especially in SiO_2 (60–92%) and Al_2O_3 (0.5–6%), was analyzed according to ASTM C114 [82]. The standard deviation below 2% minimized the impact of these variations on

uniformity; rice husk ash (RHA), with its high SiO_2 content (92%), demonstrated excellent PAI reproducibility (coefficient of variation <1%), while the higher Al_2O_3 variability in pine fiber ash (PFA, 6%) slightly increased SD (±1.5%) but did not significantly affect repeatability, owing to controlled combustion (600°C) and grinding (<45 μm). All ashes exceeded the 75% threshold required for Class N pozzolans, with PAI values ranging from 85% (PFA) to 112% (RHA) (**Table. 8**). This confirms their capability to form secondary C–S–H phases through reaction with $Ca(OH)_2$, which is attributed to their high amorphous SiO_2 content. Compositional variations influenced reactivity: higher SiO_2 content accelerated pozzolanic reactions and reduced porosity (by 15–25%, based on MIP analysis), while increased Al_2O_3 limited ettringite formation but enhanced thermal properties through higher porosity (up to 39% in PFA).

Table 7. Physical Properties of Agricultural By-Product Ashes

Raw Material	Particle Size (μm)	Surface Area (m^2/g)	Bulk Density (g/cm^3)	Porosity (%)	Water Absorption (%)	Thermal Conductivity (W/m·K)	Compressive Strength (MPa)	Tensile Strength (MPa)	Thermal Transmittance Coefficient ($W/m^2·K$)	Sieve Size (mm)
Rice Husk	23	8	1.2	18	5	0.1	2.6	0.05	0.5	0.075
Peanut Shell	53	13	1.5	23	7	0.2	2.3	0.07	0.7	0.075
Sugarcane Bagasse	73	9	1.4	21	16	0.2	1.7	0.09	0.8	0.075
Date Palm Fiber	112	14	1.3	34	23	0.2	0.8	0.001	0.9	0.075
Corn Stalk	36	12	1.4	21	9	0.3	1.5	0.001	1.1	0.075
Wheat Straw	34	15	1.6	20	12	0.3	1.2	0.001	1.2	0.075
Cotton Stalk	83	10	1.7	22	16	0.2	2.4	0.08	1.0	0.075
Soybean Husk	28	12	1.8	27	10	0.1	2.1	0.09	0.4	0.075
Pine Tree Fiber	125	15	1.9	39	24	0.3	1.1	0.001	1.3	0.075

Table 8. Key Physical and Pozzolanic Properties of Silica-Based Agricultural Ashes Used in the Study

Ash Type	Specific Surface Area (SSA, m^2/g) [BET Method]	Particle Size Distribution (PSD, μm) [D10 / D50 / D90]	Pozzolanic Activity Index (PAI, %) [ASTM C311[67]]
(RHA)	45.2 ± 2.1	1.2 / 6.5 / 18.3	112
(PNSA)	32.8 ± 1.5	2.1 / 8.2 / 22.4	98
(SCBA)	38.5 ± 1.8	1.5 / 7.1 / 19.6	105
(DPFA)	29.4 ± 1.3	2.5 / 9.0 / 24.1	92
(CSA)	35.1 ± 1.7	1.8 / 7.5 / 20.2	101
(WSA)	31.6 ± 1.4	2.3 / 8.5 / 23.0	95
(CoSA)	27.9 ± 1.2	2.8 / 9.3 / 25.5	89
(SHA)	42.3 ± 2.0	1.4 / 6.8 / 18.9	108
(PFA)	26.5 ± 1.1	3.0 / 9.8 / 26.2	85

Technical analysis of **Table. 8** shows that the highest SSA values belong to RHA (45.2 ± 2.1 m^2/g) and SHA (42.3 ± 2.0 m^2/g), with corresponding PAI values of 112% and 108% and D_{50} less than 7 μm, indicating strong pozzolanic activity, reduced permeability (20–30% for RHA), and lower thermal conductivity (up to 15% for SHA). SCBA (38.5 ± 1.8 m^2/g, PAI 105%) and CSA (35.1 ± 1.7 m^2/g, PAI 101%) exhibited a balanced performance between reactivity and workability, enhancing flowability by 5–10%. In contrast, PFA (26.5 ± 1.1 m^2/g, PAI 85%) and CoSA (27.9 ± 1.2 m^2/g, PAI 89%) were more suitable for 10–20% replacement, improving crack resistance with a slight reduction in compressive strength. The low standard deviation values (±1.1 to ±2.1) confirm the precision of the results. The

ashes were ground to pass a 45 μm sieve. The increase in SSA promoted faster formation of C–S–H gel, reduced porosity, and improved adhesion; meanwhile, the PSD with D_{50} less than 10 μm enhanced particle packing under UHPC's low water-to-binder ratio. Finally, PAI values above 75% ensured the effective performance of Class N pozzolans.

2.2 Mix Design of UHPC with and without Ash

The mix designs of UHPC with and without ash were investigated and compared, aiming to achieve high workability and compressive strength. In all mix designs, additives and pozzolanic materials such as Calimora nano-silica, silica sand, and metakaolin were incorporated. Agricultural-Origin Silica-based Ash Powder (AOSAP), was added as a percentage of the cement weight, with an equivalent amount of cement reduced. This study evaluated 28 mix designs, including mixtures with varying ash contents (0%, 10%, 20%, and 30% by weight of cement). The detailed specifications of these designs are presented in Table 8. All mix designs were implemented in accordance with ACI 211 [65] standards to ensure proper evaluation of the mixes. In the aforementioned table, the weight percentage of each component (cement, water, ash, nano-silica, metakaolin, and silica sand) in each mix design is provided. To calculate the amount of cement (C) and (AOSAP) based on the replacement percentage, the following formulas were used:

$$\left(\frac{AOSAP\%}{100}-1\right)\times C_{tatol}=C_{eff} \tag{2}$$

$$\left(\frac{AOSAP\%}{100}-1\right)\times C_{tatol}=AOSAP \tag{3}$$

Based on this formula, C_{eff}, Cement fraction replaced by Ash (kg/m^3), C_{total} amount of cement (kg/m^3), *AOSAP%* percentage of ash replacement, AOSAP amount of ash (kg/m^3).

The water-to-binder ratio (w/b) ranged from 0.18 to 0.22, which is typical for UHPC to ensure high strength and durability. The water content in all mixtures was fixed at 120 kg/m^3, and the total binder was defined as the sum of cement, fly ash, metakaolin, and nanosilica. This resulted in a slight increase in the effective water-to-binder ratio with decreasing cement (e.g., from 0.141 for 0% UHPC to 0.202 for 30% UHPCWA), calculated as water/(cement + fly ash + metakaolin + nanosilica) (see **Table. 9** and **Fig. 3)**.

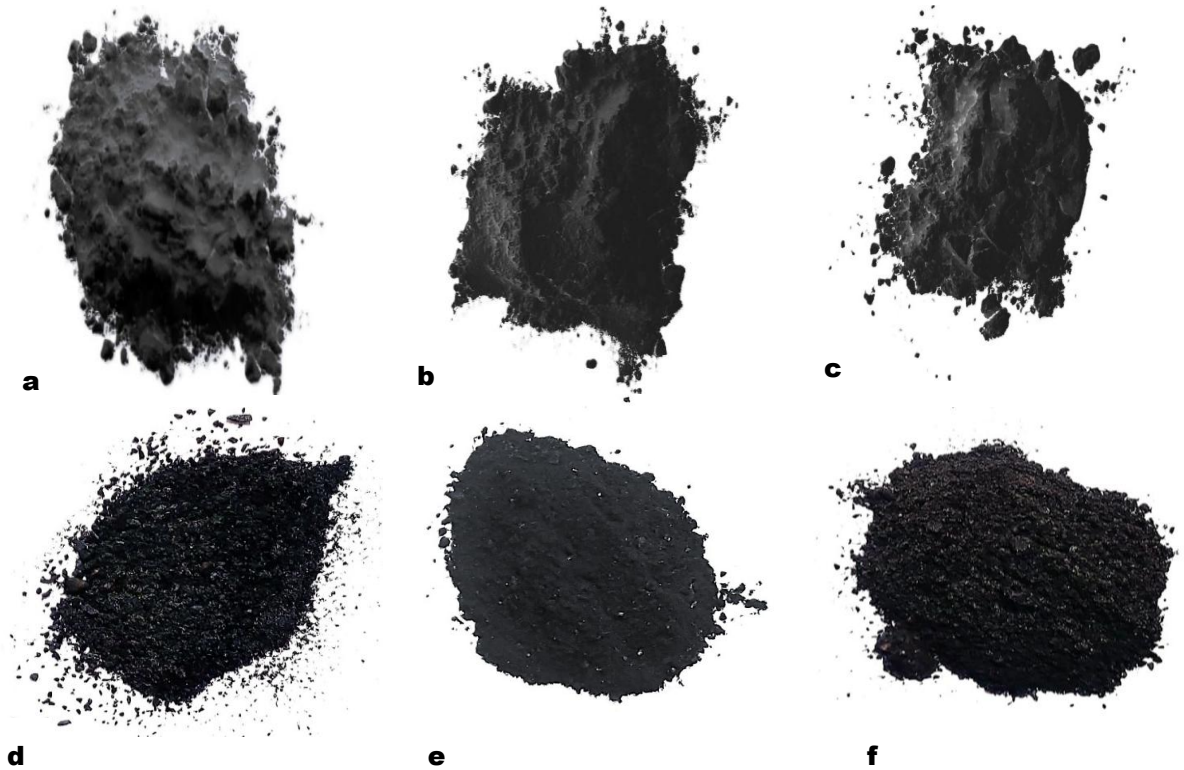

Fig. 3. Materials used in the ultra-high-strength concrete mix design: (a) Soybean Husk Ash (SHA); (b) Sugarcane Bagasse Ash (SCBA); (c) Cotton Stalk Ash (CSHA); (d) Rice Husk Ash (RHA); (e) Date Palm Fiber Ash (DPFA); (f) Pine Tree Fiber Ash (PTFA); (g) Corn Stalk Ash (CSA); (h) Peanut Shell Ash (PNSA); (i) Wheat Straw Ash (WSA); (j) Type II Portland Cement; (k) Silica Sand Fine Aggregates; (l) Calimura Nano-Silica Gel; (m) Metakaolin; (n) Water

Table 9. Mixing Plan of High Strength Concrete with and without Silica Ash

Concrete Mix	Cement (kg/m³)	Fine Aggregates (Silica Sand) (kg/m³)	Calimora Nano Silica Gel (kg/m³)	Water (kg/m³)	Metakaolin (kg/m³)	Silica Ash (kg/m³)	Superplasticizer (% of Binder)	Effective *w*/*b* Ratio
UHPC without Ash (UHPC 0%)	850 (35.41 %)	1210 (50.43%)	20 (0.83%)	120 (5%)	200 (8.33%)	0	1.5%	0.141
UHPC with 10% Ash (UHPCWA 10%)	765 (31.87 %)	1210 (50.43%)	20 (0.83%)	120 (5%)	200 (8.33%)	85 (3.54%)	1.6%	0.157
UHPC with 20% Ash (UHPCWA 20%)	680 (28.33 %)	1210 (50.43%)	20 (0.83%)	120 (5%)	200 (8.33%)	170 (7.08%)	1.8%	0.176
UHPC with 30% Ash (UHPCWA 30%)	595 (24.79 %)	1210 (50.43%)	20 (0.83%)	120 (5%)	200 (8.33%)	255 (10.62 %)	2.0%	0.202

2.3 Specimen Structure and Preparation

The specimens used in this study for evaluating the mechanical and durability properties of UHPC were designed by partially replacing cement with silica-rich agricultural waste ashes, including (RHA), (PNSA), (CSHA), (SCBA), (SHA), (CSA), (WSA), (PTFA), and (DPFA). The following sections describe the specimen structure, preparation process, and quantitative characteristics in detail.

2.3.1 Mixing and Casting

UHPC mixtures were prepared using a 50 L high-shear mixer to ensure uniform dispersion of fine particles and complete homogeneity. All materials were accurately weighed before mixing. Initially, a small amount of water was used to moisten the inner surface of the mixer, followed by the addition of silica sand and part of the mixing water to achieve complete wetting of the aggregates. Subsequently, dry materials including cement, microsilica, nanosilica, metakaolin, and agricultural ashes were added and mixed for 2 minutes at 30 rpm in dry condition to obtain a homogeneous powder blend. Next, the remaining water and superplasticizer were gradually introduced, and mixing continued for 3 minutes at 40 rpm, followed by an additional 5 minutes at 60 rpm to ensure uniform dispersion and a cohesive UHPC matrix. After complete mixing, the fresh UHPC was ready for casting. If no ash was added, the mixture represented the control sample (UHPC without ash). Tests for fresh concrete properties including slump flow, J-ring, L-box, U-box, and V-funnel were conducted for each mix design from a single batch. The optimal ash replacement range (0–30%) was determined based on detailed rheological assessments to ensure compliance with UHPC and self-compacting concrete standards. Mixtures containing 35–40% ash failed to meet the required limits (e.g., slump flow < 700 mm, V-funnel time > 12 s), indicating excessive viscosity and reduced workability. Consequently, the 30% replacement level was identified as the optimal performance threshold, balancing enhanced compressive strength with a 28.3% increase in flow time.

All mixing and casting operations were conducted under controlled environmental conditions: temperature 23 ± 1 °C, wind speed 2 km/h, relative humidity 10%, and air quality index (AQI) 45 (Good), ensuring uniformity and stability of the fresh concrete behavior.

2.3.2 Dimensions and Geometry

Cylindrical specimens with a diameter of 150 mm and a height of 300 mm were prepared for tensile strength and modulus of elasticity tests in accordance with relevant ASTM standards. Cubic specimens measuring 150×150×150 mm were cast for compressive strength, permeability, freeze–thaw resistance, ion penetration, and thermal conductivity tests. Fresh UHPC was poured into molds in two layers, and each layer was compacted on a vibration table for 30 seconds to eliminate air voids, following ASTM C192 procedures.

2.3.3 Testing Procedures

After 28 and 90 days of curing, various tests were performed on the UHPC mixtures, including:

Compressive Strength Test: ASTM C109/C109M-20 [65]

Tensile Strength Test: ASTM C496 [66]

Permeability Test: ASTM C1646/C1646M-24 [76]

Thermal Conductivity Test: ASTM C177-19 [77]

Modulus of Elasticity Test: ASTM C469 [78]

Freeze–Thaw Cycle Test: ASTM C666 [79]

Chloride Ion Penetration Test: ASTM C1202 [80]

Sulfate Resistance Test: ASTM C1012 [81]

These tests were conducted to evaluate the overall performance of UHPC under diverse conditions and to assess the influence of different ashes on its mechanical behavior and long-term durability.

2.3.4 Specimen Labeling and Replication

Each mix design, with ash replacement levels of 0%, 10%, 20%, and 30%, was replicated three

times for each type of test across the nine ashes, resulting in a total of 1000 specimens (including 108 cylindrical and 892 cubic samples). Specifically, 12 cylinders were tested for tensile strength and modulus of elasticity at each ash level, while 28 cubes were tested for compressive strength, permeability, hardened weight, freeze–thaw resistance, ion penetration, and thermal conductivity. Additional samples were prepared for fresh property evaluations. All specimens were labeled using an identification code (e.g., RHA-10 + date) to enable precise tracking during testing.

2.3.5 Curing Conditions

After casting, the specimens were covered with plastic sheets and stored for 24 hours at room temperature (23 °C) to prevent moisture loss. They were then demolded and placed in a water-curing tank at 23 ± 2 °C for 28 and 90 days, following ASTM C511, to assess both early-age and long-term performance. This structured and quantitative methodology ensured uniformity, consistency, and statistical reliability across all 1000 specimens, enabling a precise evaluation of the effects of agricultural ashes on the performance and durability of UHPC.

3 Evaluation and Analysis of Fresh Properties of UHPC with and without Ashes

Fresh properties tests were conducted to evaluate and analyze the workability and fluidity of UHPC incorporating ashes such as rice husk ash, peanut shell ash, sugarcane bagasse ash, date palm fiber, corn stalk, wheat straw, cotton stalk, soybean husk, and pine tree fiber. These materials were selected for their unique characteristics and their direct impact on the rheological and mechanical performance of the concrete. To assess parameters such as flowability, rebar passing ability, mixture stability, and preventing segregation of aggregates, fresh concrete tests were performed.

3.1 L-Box Test

The aim of this test is to assess the ability of fresh concrete to pass through obstacles (reinforcement bars) without segregation. This test emphasizes the workability of the concrete and its ability to flow through barriers without getting stuck. The L-Box consists of two sections: a vertical container for pouring concrete and a horizontal container with simulated reinforcement bars. The concrete flows from the vertical section to the horizontal section, and the ratio of the height of concrete in the horizontal section (H_2) to the height of concrete in the vertical section (H_1) is calculated. The ratio of H_2/H_1 indicates the ability of the concrete to pass through the reinforcement bars. Based on the obtained results, this ratio for UHPC with and without ash ranged from 0.8 to 1.0, where a ratio of 1.0 represents complete and unobstructed flow. This test was conducted according to EN 12350-10 [66] and EFNARC [67] standards.

3.2 U-Box Test

The aim of this test is to evaluate the filling ability and flow of concrete through rebar networks. Fresh concrete is poured into a U-shaped box that contains a reinforcement grid in the middle. Concrete flows from one U-section to the other, and the height difference of the concrete in both sections of the box is measured. This difference indicates the concrete's ability to fill the space and pass through the obstacles without segregation. The results obtained for ultra-high-performance concrete with and without ash showed a height difference of less than 30 mm, ensuring good filling and flowability of the concrete. This test was performed according to EN 12350-11[66].

3.3 J-Ring Test

The purpose of this test is to evaluate the passing ability and workability of concrete through simulated obstacles (reinforcement bars), which is typically used as a combined test with the slump flow test. Concrete is placed in a slump cone, and a J-ring, consisting of circularly arranged reinforcement bars, is positioned around the cone. After the cone is removed, the concrete flows, and the flow diameter and the height difference of concrete inside and outside the ring are measured. This height difference indicates the ability of the concrete to pass through the reinforcement bars without segregation. The results obtained for UHPC with and without ash showed a height difference of less than 10 mm, ensuring proper passability of the concrete. This test was conducted according to ASTM C1621/C1621M [69] and EN 12350-12 [70] standards.

3.4 Slump Flow Test

The aim of this evaluation is to assess the workability of UHPC and its ability to fill molds without the need for vibration. This test is the most important criterion for evaluating the fluidity and stability of fresh concrete mixes. Fresh concrete is poured into a standard slump cone, and the cone is then removed. The diameter of the concrete spread on a flat surface is measured. This flow diameter represents the fluidity of the concrete. Based on the obtained results for UHPC with and without ash, the slump flow diameter ranged from 735 to 750 mm. A flow less than 600 mm indicates insufficient fluidity, while a flow greater than 800 mm may indicate material segregation. This test was conducted according to ASTM C1611/C1611M [71], and EN 12350-8 [72] standards.

3.5 V-Box Test

The aim of this evaluation is to assess the viscosity and flow rate of UHPC. This test helps evaluate the concrete's ability to flow through obstacles without delay and segregation. Fresh concrete is poured into a V-shaped funnel, and the total discharge time (the time taken for the concrete to pass through the funnel) is measured. A longer discharge time indicates higher viscosity and greater resistance to flow. Based on the results obtained for UHPC with and without ash, the discharge time ranged from 3 to 5 seconds. A discharge time greater than 12 seconds indicates high viscosity and reduced workability of the concrete. This test was conducted according to EN 12350-9 [73] standard.

3.6 Flowability and Viscosity

UHPC exhibits high flowability and workability due to its high cement content and the incorporation of nano-silica gel. However, since UHPC has an extremely low water-to-cement (W/C) ratio, the effect of ash, due to its high amorphous silica content, which is an active pozzolan, can react with the cement to produce more gel products. The addition of ash reduces viscosity and enhances the flowability of the concrete.

3.7 Stability and Segregation Resistance

In UHPC, the use of fine materials such as nano-silica and metakaolin improves the stability of the mix and prevents material segregation in the fresh state. Segregation typically occurs due to differences in the specific gravity of the materials. The effect of ash, with its extremely fine particle structure and active pozzolanic surface, helps fill the voids between cement particles, reducing the risk of segregation in UHPC. UHPC exhibits a shorter setting time due to the use of nano-silica. This characteristic is particularly beneficial for structures that require rapid loading. Due to its high density and the use of additives, UHPC has good passing ability through reinforced steel networks. The presence of ash can significantly improve this passing ability. In general, UHPC has a significantly lower tendency to bleed due to its very fine particle size distribution and low water-to-cement ratio. The effect of ash, with its high surface area and pozzolanic activity, can absorb excess water and minimize bleeding. The use of agricultural ash in UHPC can provide numerous advantages in improving the fresh properties of the concrete, including enhanced stability, better filling ability, reduced bleeding, and controlled setting time. These tests serve as tools for evaluating the rheological properties of fresh concrete. The use of these methods, in accordance with established standards, ensures that the concrete is suitable in terms of flowability, passing ability through reinforcement, and mix stability for specific applications. The test results are shown in **Fig. 4**.

4 Investigation and Analysis of the Hardened Properties of UHPC with and without Ashes

The hardened properties of UHPC were examined using a variety of ashes, including rice husk ash, peanut shell ash, sugarcane bagasse ash, palm tree fiber ash, corn stalk ash, wheat straw ash, cotton stalk ash, soybean husk ash, and pine tree fiber ash. These materials were selected due to their unique characteristics and their direct influence on the rheological and mechanical performance of concrete.

4.1 Analysis of Compressive Strength Results

Compressive strength, a pivotal mechanical property of UHPC, was rigorously evaluated through

testing of specimens at 28 and 90 days, including both control samples and those incorporating varying ash contents. The results highlight a significant enhancement in compressive strength attributable to ash addition, establishing it as a viable strategy for optimizing the mechanical performance of pozzolanic concretes. Tests were conducted in accordance with ISIRI 3206 [74] standards on 150×150×150 mm cubic specimens, with detailed outcomes presented in **Fig. 5**. The observed strength gains in UHPC are driven by the chemical reactivity of ash components, which interact with hydration products to foster a denser, more cohesive microstructure. This enhancement is facilitated by the reactive constituents within the ashes, engaging with hydration byproducts to refine the internal matrix and strengthen interfacial bonding, thereby bolstering overall structural integrity.

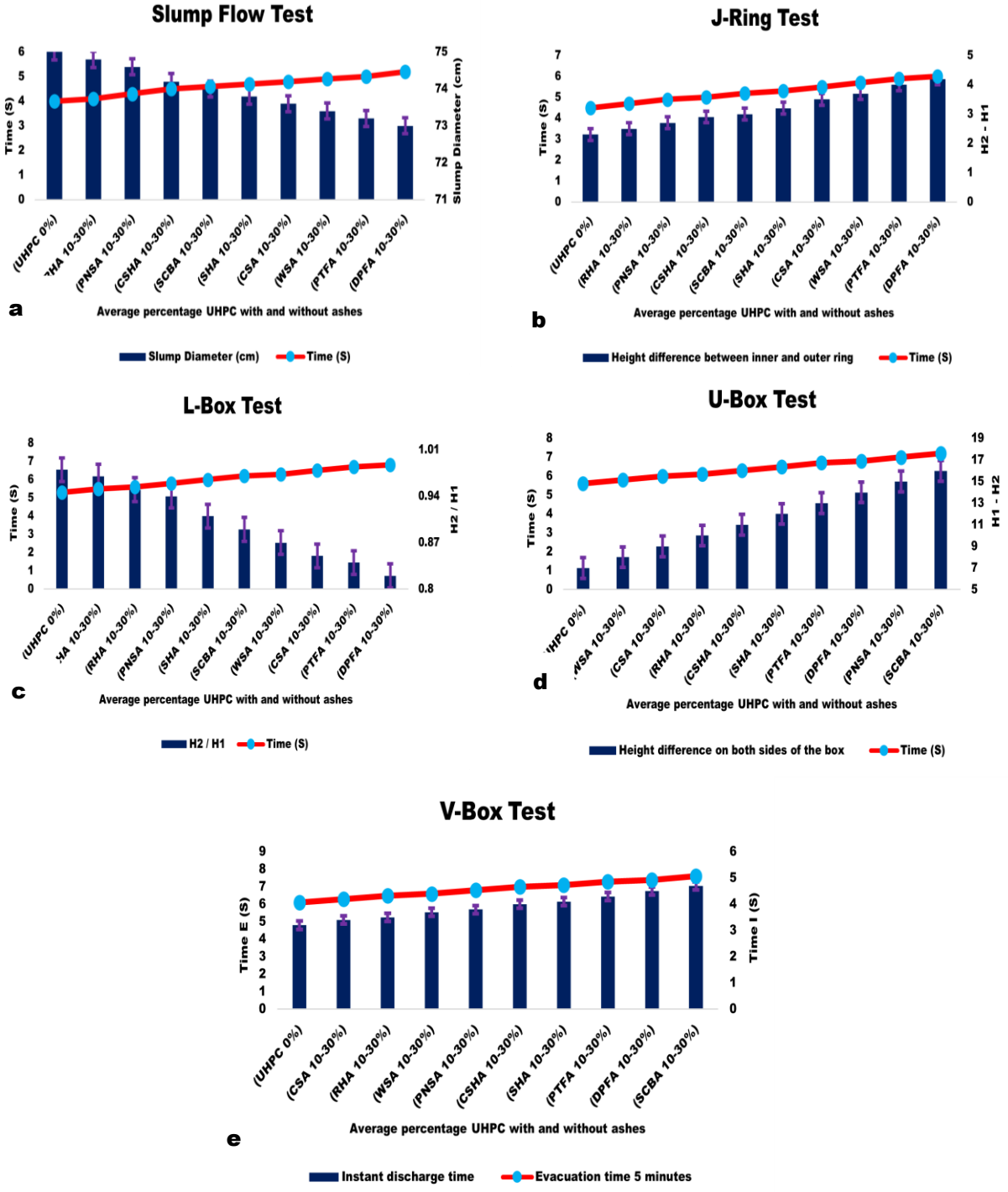

Fig. 4. Results and evaluation of the fresh properties of UHPC with and without ash; a) Slump flow test b) J-ring test c) L-box test d) U-box test e) V-box test

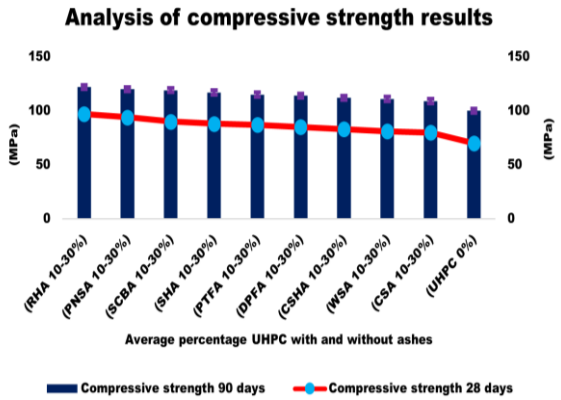

Fig. 5. Evaluation and Results of Compressive Strength of (UHPC) with and without Ashes

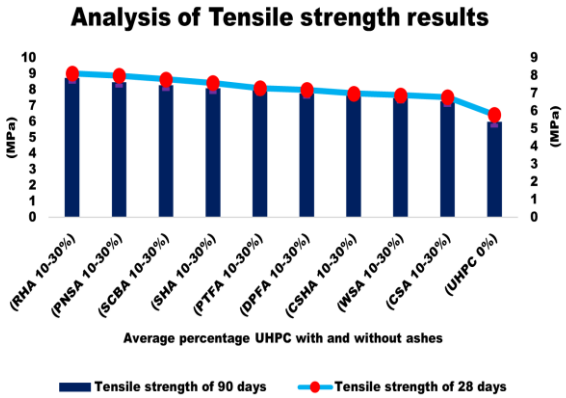

Fig. 6. Evaluation and Results of the Tensile Strength of (UHPC) With and Without Ashes

4.2 Analysis of Tensile Strength Results

Tensile strength, a critical mechanical characteristic of (UHPC), was systematically assessed through experiments conducted on specimens at 28 and 90 days, encompassing both reference samples and those with varying ash incorporations. The findings, detailed in **Fig. 6**, reveal a notable increase in tensile strength across all tested ages due to ash integration, underscoring its efficacy in enhancing the mechanical properties of pozzolanic concretes. Tensile strength evaluation was performed on cylindrical specimens (150×300 mm) according to ASTM C496 [75]. The synergy of nano silica with ashes further amplifies this improvement, highlighting a promising approach for material optimization. This enhancement stems from the reactive nature of silica-based ashes and pozzolanic additives, such as metakaolin and nano silica, which, owing to their amorphous silica content, engage in pozzolanic reactions within the concrete's alkaline milieu. These reactions, facilitated by $(Ca(OH)_2)$ from cement hydration, generate secondary products that reinforce the matrix, improving cohesion and densifying weak interfacial zones, thereby substantially elevating tensile strength.

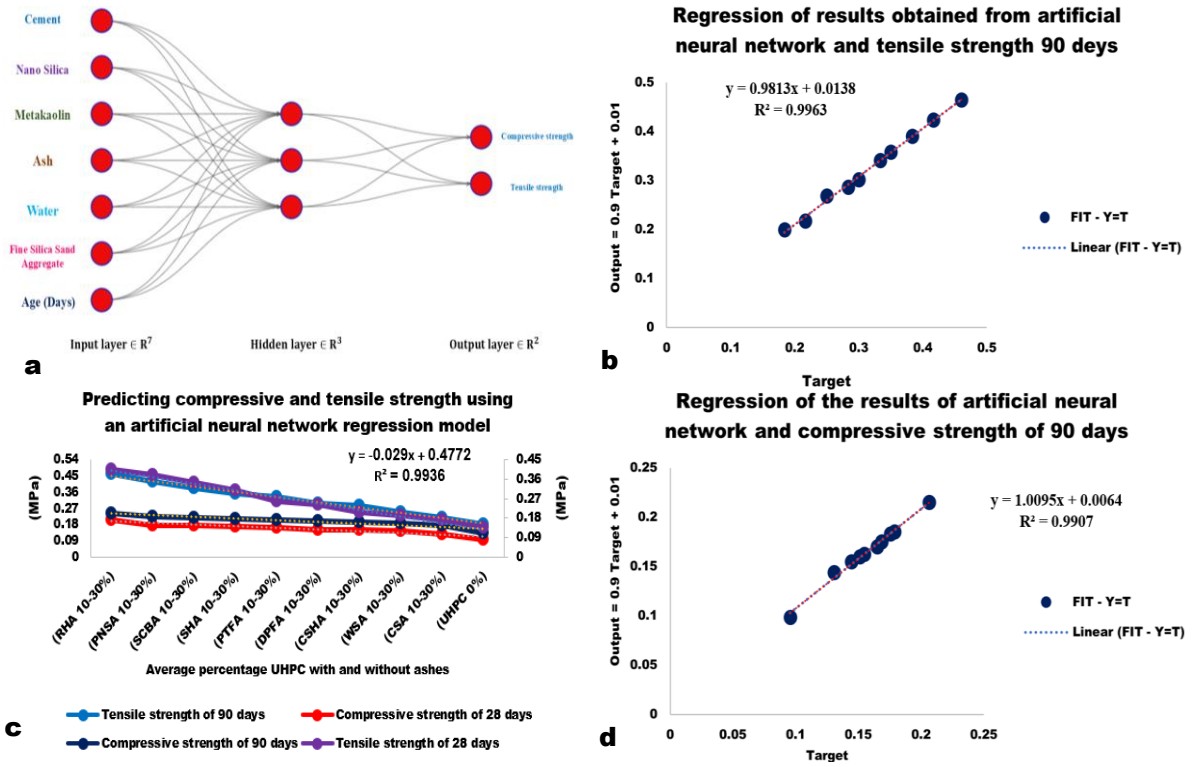

Fig. 7. (a) Artificial neural network structure for predicting compressive and tensile strength, (b) Regression results obtained from the artificial neural network for estimating tensile strength, (c) Correlation between 28-day and 90-day tensile and compressive strength predicted by the artificial neural network, (d) Regression results obtained from the artificial neural network for estimating compressive strength

4.3 Artificial Neural Network Structure

Table 10. Variables considered in the artificial neural network and specifications of the optimized neural network model

Variable (kg/m³)	Min	Max	Average	SD	MAE (MPa)	RMSE (MPa)	Cross-Validation Loss (%)	R^2	Training Time (min)	Model Complexity (Parameters)	Learning Rate	Batch Size	Training/Test Split (%)
Neural Network (MLP)													
Input													
Age (days)	28	90	59	1.23	-	-	-	-	-	-	0.01	32	70/30
Portland Cement Type 2	855	600	725.5	3.88	-	-	-	-	-	-	0.01	32	70/30
Fine Aggregate (Silica Sand)	-	1210	-	-	-	-	-	-	-	-	0.01	32	70/30
Calimora Nano-Silica Gel	-	20	-	-	-	-	-	-	-	-	0.01	32	70/30
Water	-	120	-	-	-	-	-	-	-	-	0.01	32	70/30
Metakaolin	-	200	-	-	-	-	-	-	-	-	0.01	32	70/30
Ash (AOSAP)	90	260	175	2.55	-	-	-	-	-	-	0.01	32	70/30
Output													
Compressive Strength (MPa)	70	122	96	1.08	1.25	1.85	2.1	0.99	45	15000	0.01	32	70/30
Tensile Strength (MPa)	6.01	9.2	7.6	3.15	0.18	0.25	2.1	0.99	46	15000	0.01	32	70/30

A Multilayer Perceptron (MLP) neural network, comprising input, hidden, and output layers, was employed to model the complex, nonlinear relationships between mix parameters and the compressive and tensile strengths of UHPC. This feedforward architecture utilized activation functions Tansig (hidden layers) and Purelin (input/output layers) to capture these relationships, with learning facilitated by the Levenberg-Marquardt backpropagation algorithm over 169 iterations. Input variables were selected based on their significant impact on UHPC strength, determined through correlation analysis (Pearson's $r > 0.7$) and stepwise regression from an initial pool of 12 variables. The finalized inputs included Age (28–90 days), Portland Cement Type 2 (600–855 kg/m³), Fine Silica Sand Aggregate (up to 1210 kg/m³), Calimora Nano Silica Gel (up to 20 kg/m³), Water (up to 120 kg/m³), Metakaolin (up to 200 kg/m³), and Ash (90–260 kg/m³), chosen for their high explanatory power ($R^2 > 0.85$) and alignment with prior research (e.g., Endale et al., 2023 [28]). The optimal MLP structure, illustrated in **Fig. 7a**, features seven input neurons, 21 hidden neurons, and two output neurons, refined using cross-validation (k=5 folds) and grid search. Overfitting was mitigated via L_2 regularization (penalty factor 0.01), dropout (rate 0.2), and early stopping (patience 10 epochs), tailored to the dataset's quality and computational resources. The 28-mix dataset was split into 70% training and 30% testing, with 10 independent trials ensuring robustness. Data normalization using the Z-score method standardized inputs, enhancing convergence within a Deep Neural Network (DNN) framework integrated with Full Factorial Design-based Response Surface Methodology (RSMFFD). Comprehensive statistical analyses on input data, detailed in **Table. 10**, guided the initial structure and activation function selection. The performance of the optimized MLP, depicted in **Fig. 7c**, was evaluated using linear regression, achieving a correlation coefficient (R^2) of 0.99, indicating statistically significant agreement with experimental data ($p < 0.01$, SD = 1.08 MPa for compressive strength, 3.15 MPa for tensile strength). Validation metrics included Mean Absolute Error (MAE) of 1.25 MPa (compressive) and 0.18 MPa (tensile), Root Mean Square Error (RMSE) of 1.85 MPa and 0.25 MPa, respectively, and Mean Absolute Percentage Error (MAPE) of 1.2%. Cross-validation yielded an average loss of 2.1% ($p < 0.05$), confirming robustness. **Figs. 7b–7d** compare predicted and actual outputs, with Analysis of Variance (ANOVA) and t-tests validating improvements. Sensitivity analysis highlighted ash content (40%) and curing age (25%) as primary variance contributors, with triplicate testing (CV <2%) ensuring repeatability despite ±5% SiO_2 variability.

4.4 Analysis of Elastic Modulus Results

The elastic modulus, a crucial mechanical attribute of UHPC, was systematically investigated as part of this study, with experiments conducted at 28 and 90 days on both reference samples and those blended with varying ash proportions. As illustrated in **Fig. 8**, the incorporation of ash as a partial replacement for cement resulted in a significant enhancement of the elastic modulus at all tested ages, demonstrating its positive contribution to the overall mechanical performance of UHPC. The elastic modulus evaluation was performed on cylindrical specimens (150×300 mm) according to ASTM C469 [78]. This enhancement is attributed to the reactive nature of silica-based ashes and pozzolanic additives, including metakaolin and nano silica, which, due to their amorphous silica composition and organic constituents, trigger pozzolanic interactions within the concrete's alkaline setting. These interactions, especially in the presence of ($Ca(OH)_2$), facilitate the development of secondary products that enhance matrix cohesion and density. The resulting fortified microstructure reinforces weaker zones and strengthens the interfacial connections among cement particles, significantly boosting the elastic modulus of the concrete.

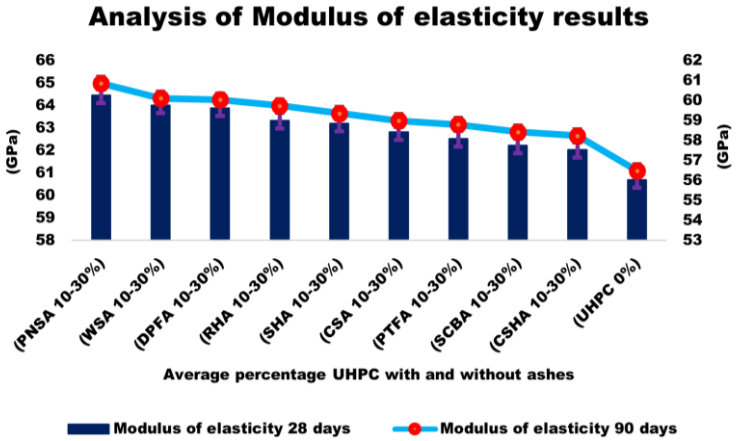

Fig. 8. Evaluation and results of the elastic modulus of UHPC with and without ashes

4.5 Durability and Freeze-Thaw Resistance of UHPC

One of the key aspects in evaluating the durability of UHPC is its resistance to freeze-thaw cycles, particularly critical in cold climates, where repeated freezing and thawing of pore water can induce cracking and structural damage. The incorporation of various ashes as additives and pozzolans in UHPC enhances both mechanical properties and durability by reducing permeability and densifying the microstructure. In this study, cubic samples of UHPC with ash replacements ([RHA], [PNSA], [SCBA], [SHA], [PTFA], [DPFA], [CSHA], [WSA], and [CSA] at 10–30%) were prepared and cured for 28 days under standard conditions (23°C, >95% RH). The samples underwent 30 freeze-thaw cycles, consisting of freezing at -18°C for 24 hours followed by thawing at 20°C for 24 hours. Weight loss and compressive strength were measured before and after testing, with results presented in **Fig. 9**. Compared to the reference mix (UHPC 0% ash), which exhibited an initial compressive strength of 70 MPa, dropping to 53 MPa (24% reduction) and a hardened weight of 22 kg with ~5% mass loss after 30 cycles, ash incorporation markedly improved freeze-thaw resistance. RHA mixes achieved an initial strength of 97 MPa, retaining 79 MPa (18.6% reduction) with a hardened weight of 24.3 kg and <1% mass loss, attributable to high amorphous SiO_2 (>80%) enhancing C-S-H density and reducing permeability. PNSA and SCBA mixes recorded initial strengths of 94 MPa and 90 MPa, retaining 77 MPa and 76 MPa (18.1% and 15.6% reductions), respectively, with weights of 24.1 kg and 23.9 kg, reflecting moderate SiO_2 (65–70%) and pore refinement (15–20%). CSA, with an initial 80 MPa and post-cycle 62 MPa (22.5% reduction), and a weight of 22.7 kg, showed less resistance due to higher porosity (25–30%) and lower SiO_2 (~60%). Sulfate resistance was evaluated by immersing samples in a 5% Sodium sulfate (Na_2SO_4) solution for 28 days, with the reference mix dropping from 70 MPa to 45 MPa (36% reduction) due to ettringite and gypsum formation. Ash addition improved resistance significantly. RHA mixes retained 72 MPa (25.8% reduction from 97 MPa), a 60% improvement over the reference, driven by SiO_2 densification and Al_2O_3 (10–12%) stabilizing reaction products. PNSA and SCBA retained 70 MPa and 68 MPa (25.5% and 24.4% reductions), while CSA retained 55 MPa

(31.3% reduction), reflecting lower Al_2O_3 (~6%) and higher porosity. These enhancements correlate with pozzolanic activity and reduced permeability, with triplicate testing (CV <2%) ensuring consistency. The synergy between nanosilica, metakaolin, and ash significantly enhanced performance. The reference mix (UHPC 0%) decreased from 70 MPa to 53 MPa (a 24% reduction) with a 5% mass loss. The RHA mixes incorporating nanosilica and metakaolin maintained 79 MPa (an 18.6% reduction) and less than 0.5% strength loss, attributed to the early C–S–H nucleation by nanosilica, the long-term pozzolanic reaction of metakaolin, and the pore-filling effect of ash (resulting in a 55–66% reduction in permeability). The combination of metakaolin and ash (SiO_2 60–85%, Al_2O_3 5–15%) enhances long-term pozzolanic reactivity.

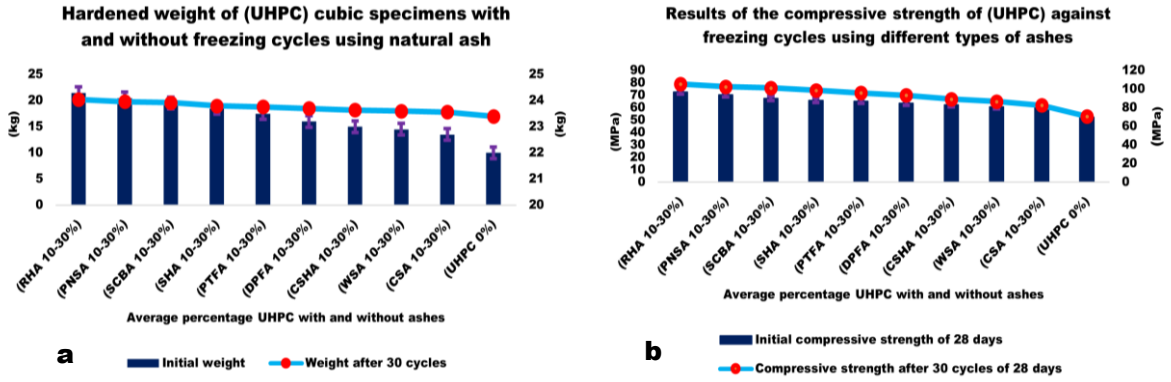

Fig. 9. Evaluation and Results: (a) Compressive Strength (b) Hardened Weight Against Freeze-Thaw Cycles of UHPC with and without Ashes

4.6 Permeability Test

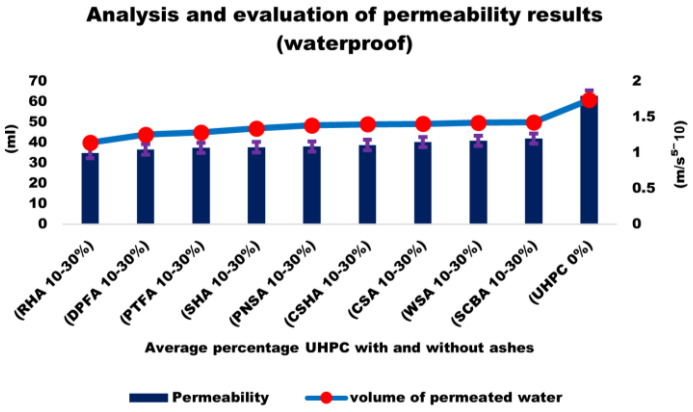

Fig. 10. Evaluation and Results of the Permeability of UHPC with and without Ashes

UHPC is considered one of the advanced options in the construction industry due to its exceptional physical and mechanical properties. The permeability of this type of concrete is particularly critical in humid environmental conditions and when in contact with corrosive ions. This study investigates the effect of bio-ashes on the water permeability under pressure. For the experiment, cubic samples with dimensions of 150×150×150 mm are removed from the molds after 24 hours and cured in clean water for 28 days. The water permeability under pressure test is conducted using a waterproof device. The samples are placed in a chamber where water at a specified pressure of 1 MPa is applied, in accordance with the BS EN 12390-8 standard [82]. The duration of the test is typically 72 hours, during which the amount of water penetrating the sample is measured. Permeability is calculated based on the volume of water that has penetrated the sample, and it is expressed using the following formula:

$$\frac{V}{A \times t} = P \tag{4}$$

where: P is the permeability (m/s), V is the volume of water that has penetrated (m^3), A is the cross-sectional area of the sample (m^2), t is the time (s). The use of bio-ashes generally leads to a reduction in the permeability of UHPC. The results of the permeability test are shown in **Fig. 10**.

4.7 Resistance to Chloride and Sulfate Ions

The resistance of UHPC to chloride and sulfate ions is a key factor in assessing its durability under harsh environmental conditions. These ions can cause degradation and reduce the service life of concrete structures. Due to its excellent mechanical properties and high durability, UHPC is widely used in construction projects and underwater structures. The use of ash as a cement additive can improve the concrete's resistance to chloride and sulfate ion attacks. After 24 hours, cubic specimens with dimensions of 150×150×150 mm are removed from the molds and cured for 28 days under controlled conditions (humidity and temperature). Following curing, the specimens are immersed in a 3% Sodium chloride (NaCl) chloride solution for a specified period of 28 days, in accordance with ASTM C1556 [82]. Similarly, the specimens are immersed in a 5% Na_2SO_4 sulfate solution according to ASTM C1012/C1012M [81] for the same duration. After the immersion period, the specimens are removed from the solutions and stored at room temperature for 24 hours to ensure that their surfaces are fully saturated and dry. The specimens are then transferred to a compressive strength testing machine, where their compressive strength is measured. The results of the UHPC's resistance to chloride and sulfate ions are presented in **Fig. 11**.

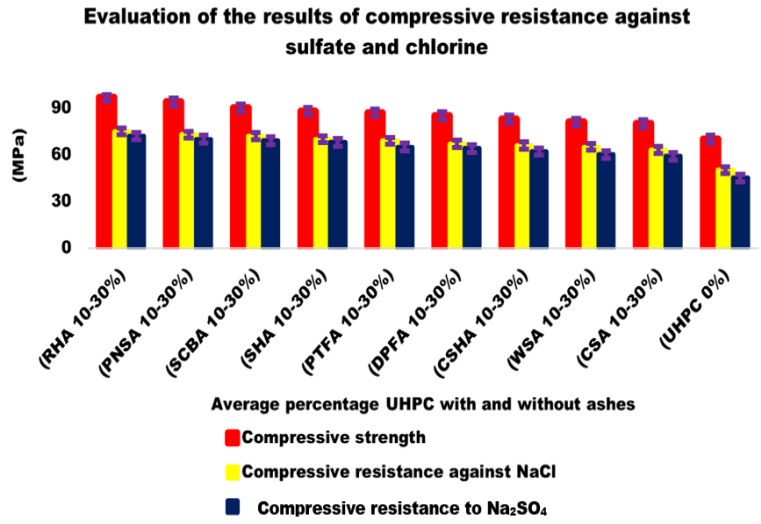

Fig. 11. Evaluation and Results of Compressive Strength Resistance to Chloride and Sulfate Ions in UHPC with and without Ashes

4.8 Thermal Conductivity Test

Thermal conductivity (λ) of UHPC is an important indicator of its ability to transfer heat, which plays a crucial role in improving the thermal performance of buildings. The use of bio-ashes (such as rice husk ash, peanut shell ash, sugarcane bagasse ash, date palm fiber, corn stalk, wheat straw, cotton stalk, soybean husk ash, and pine tree fiber) has the potential to reduce the thermal conductivity in concrete and enhance its thermal performance. The samples were prepared as cubic molds with dimensions of 150×150×150 mm and were cured for 28 days under standard conditions. After the 28-day curing period, the samples were placed in a thermal conductivity device, and a thermal sensor was directly attached to the center of the surface of each sample. A direct heat transfer method was employed, and the thermal conductivity (λ) was measured and recorded at specific temperatures. Thermal conductivity (W/m·K) serves as the primary parameter for assessing the heat-transfer ability of concrete. The temperature range for the tests was set between 20-60°C to simulate realistic environmental and field conditions, as per ASTM C177-19 [83] standards. The Hot Disk device was used with the Heat Flow Method. A defined heat flow was applied to the sensor, and simultaneous temperature changes and heat transfer data from the sensor to the sample surface were recorded. Each heat transfer test was conducted for 48 hours. During this period, the device measured the temperature increase on the surface of the sample and recorded the corresponding data. The device analyzed the recorded temperature data and, based on time, temperature, and heat transfer rate, calculated the thermal conductivity (λ) for each sample. Using standard heat transfer formulas, the recorded temperature, sample area, and testing duration were used to determine the precise thermal conductivity for each sample. The thermal

conductivity is calculated using the following equation, which is employed in tests using Heat Flow Meter devices [83]:

$$\frac{Q \times d}{A \times \Delta T} = \lambda \tag{5}$$

where: λ : Thermal conductivity of concrete (W/m·K), Q: Heat flow passing through the sample (W), d: Thickness of the sample (m), A: Cross-sectional area of the sample (m²), ΔT: Temperature difference across the sample (°C). As shown in **Fig. 12**, the results are clearly presented.

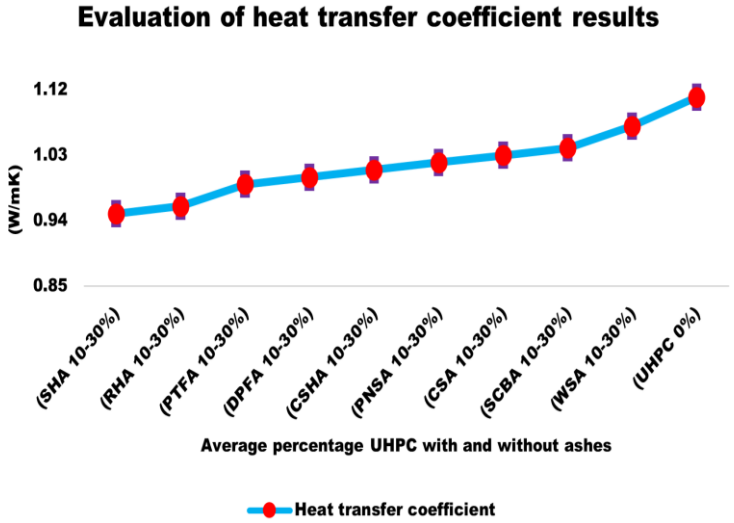

Fig. 12. Evaluation and Results of the Thermal Conductivity Test for UHPC with and without Ashes

5 Evaluation, interpretation of results, optimization and structural analysis

The use of silica-rich agricultural by-products ash in combination with cement, in addition to reducing cement consumption, leads to an improvement in the mechanical properties of concrete, including compressive strength, tensile strength, and modulus of elasticity. Furthermore, this additive enhances the durability of concrete under harsh environmental conditions, including resistance to freeze-thaw cycles, chloride and sulfate ion resistance, and a reduction in water permeability. One of the significant advantages of using ash is the reduction in the heat transfer coefficient of concrete, which can contribute to increased stability against temperature variations. These properties make ash-modified UHPC perform better in structural applications exposed to high or low temperatures. Based on the analysis of experimental results and comparison with previous studies, this research presents a comprehensive model for predicting the comparative behavior and experimental investigation of the impact of various natural ashes on the mechanical and thermal properties of UHPC.

5.1 Central Composite Design (CCD)

CCD combines factorial points (a set of different values for the variables), central points (repeated factorial points for error assessment), and axial points (points along the axes typically at a certain distance from the factorial points). This design allows for full coverage of the response space and accurate evaluation of the effects. The inclusion of axial points in CCD helps model the nonlinear effects of variables. For instance, in this study, the effect of ash replacement percentage with cement on concrete compressive strength is nonlinear. The presence of these points enables the identification of strengths and weaknesses in the design, leading to the development of accurate models for predicting the properties of concrete. The Response Surface Methodology (RSM) uses experimental data obtained from the CCD design to develop regression equations. These equations are generally second-degree polynomial types and can describe complex and nonlinear relationships between variables and concrete properties. RSM allows for the analysis of the response surface and the graphical examination of the relationships between variables and responses. Using response surface graphics, optimal regions of the design space are identified. Additionally, RSM facilitates sensitivity analysis, enabling the investigation of the impact of small changes in variable values on concrete properties. This analysis can be highly

beneficial for experiment design and cost reduction.

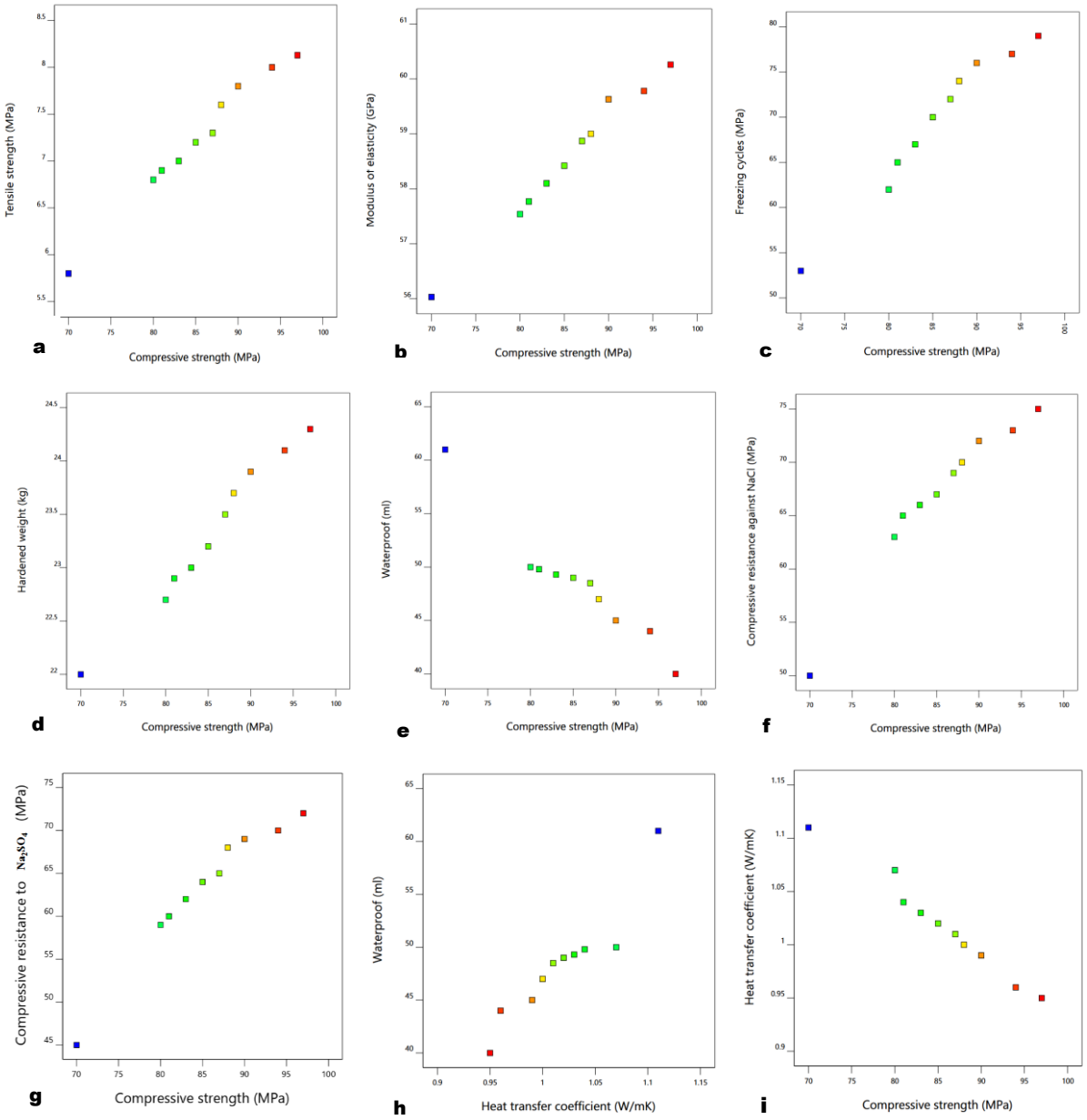

Fig. 13. Experimental results using the optimization method (RSM) Central Composite Design for UHPC with and without ashes

In **Fig. 13a**, the cement content in UHPC without ash is 850 kg/m³, which is significantly higher than in other mixes. This increase results in a reduction in compressive strength (70 MPa) and tensile strength (5.8 MPa). This decline is due to the heterogeneity of the mixture or the incomplete reaction of cement at such a high ratio. In other mixes with 595 kg/m³ cement and 127.5 kg/m³ ash, compressive and tensile strengths are improved, indicating the positive effect of ash on the cement-concrete mixture. The highest compressive strength (97 MPa) and tensile strength (8.13 MPa) were observed with rice husk ash in the UHPC mix. This increase in compressive strength is attributed to the improved dispersion of the cement and ash phases, which leads to higher density and reduced voids in the concrete's internal structure. As a pozzolanic material, ash reacts in hydration reactions, forming new hydration products that enhance the final compressive strength. The increase in tensile strength can be attributed to the ash filling micro-pores and improving the bond between particles in the concrete structure, thus enhancing the tensile capacity of the concrete. This effect is particularly important for UHPC, which requires enhanced internal bonding to withstand high tensile stresses (**Fig. 13a**). The increase in the modulus of elasticity indicates that concrete containing higher ash content has become

harder and stiffer. The modulus of elasticity for UHPC increased from 56.03 GPa in a sample with 850 kg/m³ cement (and no ash) to 60.26 GPa in a sample with 127.5 kg/m³ peanut shell ash. This increase in modulus of elasticity reflects the higher stiffness of concrete with ash. Due to its fine-grained structure and pozzolanic activity, ash can react with calcium hydroxide produced during hydration to form additional calcium silicate products, increasing the rigidity of the concrete structure. These secondary products contribute to better cohesion and reduced variability in the concrete (**Fig. 13b**). The increase in compressive strength under freeze-thaw cycles shows that concrete with higher ash content has become harder and stiffer. The compressive strength under freeze-thaw cycles for UHPC increased from 53 MPa in a sample with 850 kg/m³ cement (and no ash) to 79 MPa in a sample with rice husk ash. This is due to the higher resistance of ash to freezing conditions, resulting in improved durability of the concrete. This increase may be due to the densification and reduced permeability of the concrete, preventing water penetration and reducing freeze-induced damage (**Fig. 13c**). The weight of hardened concrete in samples containing ash (averaging 23-24 kg) is lower than in the first sample, which can be attributed to the reduction in mix density due to the addition of ash. This weight reduction may be due to the more porous and lightweight structure of the ash, contributing to a lower overall concrete density (**Fig. 13d**). Additionally, water permeability has decreased (the UHPC sample without ash dropped from 61 ml to about 49 ml with rice husk ash), indicating the positive effect of ash in improving concrete's resistance to water and reducing permeability (**Fig. 13e**). The results regarding compressive strength against chloride and sulfate ions show that samples with 127.5 kg/m³ ash performed better under final compression conditions. The compressive strength of concrete samples with ash was higher than in samples without ash, averaging from 45-50 MPa to about 72-75 MPa. These results indicate an improvement in the compressive properties of concrete in the presence of ash (**Figs. 13f** and **13g**). The heat transfer coefficient in ash-containing samples increased from 1.11 W/mK in the concrete sample without ash to 0.95 to 1.07 W/mK in concrete samples with ash, which aids in improving heat transfer in specific applications (**Figs. 13h** and **13i**). Based on the above analyses, it can be concluded that the use of ash at a fixed amount of 127.5 kg/m³ combined with 595 kg/m³ cement leads to significant improvements in compressive strength, tensile strength, modulus of elasticity, and freeze-thaw resistance. This combination also results in properties such as reduced permeability and concrete weight, making it suitable for enhancing durability and performance under various environmental conditions.

The three-dimensional surface plot (**Fig. 14a**) from the (RSM) illustrates the design standard error as a function of cement content (595 to 850 kg/m³) and ash content (0 to 260 kg/m³). It shows a low error (<0.2) in cement-rich mixtures with low ash and a nonlinear increase to >1.0 with higher ash content, confirming the model's high accuracy in cement-rich mixtures. This highlights the role of ash in increasing uncertainty due to pozzolanic variability, while still allowing up to a 15% strength gain with 30% replacement. The interaction plot (**Fig. 14b**) indicates that the standard error decreases linearly with increasing cement content at a fixed ash level (127.5 kg/m³), with a low-error point (0.2) at 595 kg/m³ cement and a high-error point (1.2) at 850 kg/m³ cement, confirming an inverse relationship ($R^2 = 0.95$). This emphasizes the efficiency of RSM in optimizing cement ash ratios.

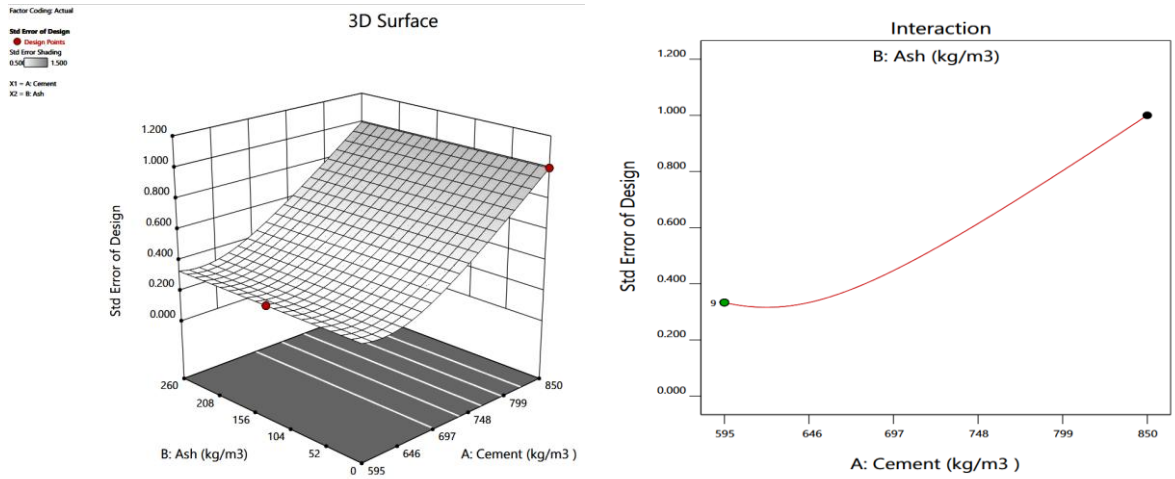

Fig. 14. Optimal effect of ashes on cement in UHPC

In the concluding summary, it should be noted that the results showed that the partial replacement of cement with natural ashes led to a significant improvement in the compressive, and tensile strength of UHPC. The increase in the modulus of elasticity is attributed to enhanced internal bonds and a reduction in voids within the concrete structure. These improvements are the result of using ash as an active pozzolanic material, which increases the density and improves the bond between the cement particles and the ash. The experiments demonstrated that the addition of ash to UHPC enhanced its durability under harsh environmental conditions. In particular, this concrete exhibited better performance against freeze-thaw cycles and prevented early spalling or cracking. Moreover, a significant reduction in permeability and an increase in resistance to chloride and sulfate ions indicated a decrease in chemical attacks and an improvement in the longevity of the concrete. These durability enhancements make ash-modified UHPC a suitable choice for structural applications in corrosive environments and regions with extreme temperature fluctuations. Another significant benefit of this research is the reduction in the thermal conductivity of this type of concrete. A lower thermal conductivity means reduced heat transfer rates in concrete structures, which can protect UHPC against thermal shocks and temperature changes, thus extending the service life of the structure. This aspect is particularly important for projects located in areas with extremely high or low temperatures. Through statistical data analysis and comparison with the results of previous studies, this research has developed and presented a comprehensive predictive model for evaluating the behavior of UHPC with various ash compositions. This model can serve as an efficient tool for predicting the mechanical properties and durability of UHPC using different natural ashes. The findings of this study can pave the way for the development of design guidelines for UHPC utilizing natural pozzolanic materials. Houet al. (2024) [7] aimed to investigate the potential of using rice husk ash (RHA) along with other pozzolans as a cement replacement, both in the stage of aggregate modification and in the production of UHPC. The UHPC produced with 30% RHA achieved a high compressive strength of 112.86 MPa, which was about 13% higher than the reference concrete. The rapid chloride permeability test Rapid Chloride Penetration Test (RCPT) and water permeability tests of the UHPC with rice husk ash also showed significant improvements compared to the reference mix. Nadesan (2018) [30] designed and tested Self-Compacting High Strength Concrete (SCHSC) concrete with rice husk ash at 0%, 10%, 20%, 30%, and 40% by weight, measuring the compressive strength of all mixes at 28 days. Based on the experimental results, the compressive strength of UHPC with 30% rice husk ash showed a 14.6% increase in strength compared to mixes without rice husk ash. Witowski et al. (2023) [14] investigated the use of rice husk ash in high-strength concrete. Silica fume was used as a control additive in the mix design. The experiments were conducted by replacing cement with rice husk ash at varying levels (0% - 35%). The results indicated that, despite the presence of silica, combining rice husk ash with silica fume resulted in a 12% increase in the compressive strength of high-strength concrete compared to the reference sample.

5.2 Deep Statistical Analysis

The hardened properties were analyzed using RSM linear model:

$Y = a + b\mathrm{bReplacement} + \mathrm{cAsh\_Code}$ under deep statistical analysis to evaluate the effects of ash on UHPC. Data for 10–30% replacement were averaged and considered as 30% for modeling purposes. The analyses included (ANOVA) (ash effect), Student's t-test (t-test) (ash vs. control), Kruskal–Wallis non-parametric test (Kruskal–Wallis test), model assumptions, regression metrics, error assessment, sensitivity analysis, outlier detection, multivariate modeling, and validation Cross-Validation (5-fold CV, 80/20 hold-out, external control points) (see **Table.11**).

RSM provides a robust statistical framework for modeling the effect of ash replacement on the compressive strength of UHPC at 28 and 90 days using a linear equation$(\mathrm{Strength} = \beta_0 + \beta_1 * \mathrm{Replacement} + \varepsilon)$Regression Coefficients (β_0, β_1), Error Term (ε). This analysis highlights significant improvements at 90 days due to pozzolanic curing, with key metrics interpreted below.

Statistical Significance: Analysis of variance (ANOVA) Probability Value, F Statistic ($p = 0.0301$, $F = 4.36$ at 28 days; $p = 0.0137$, $F = 5.78$ at 90 days) confirms model validity ($\alpha = 0.05$). The t-test ($p < 0.00001$) demonstrates the superiority of ash over control samples, with Cohen's $d > 3$ indicating a large effect size (15–20% strength increase). The Kruskal–Wallis test ($p = 0.117$), despite the small sample size ($n = 10$), corroborates the parametric findings.

Table 11. Deep analysis for compressive strength (28 and 90 days)

Category	Analysis/Details	Results (28 days)	Results (90 days)	Implications
Statistical Significance	ANOVA (ash effect), t-test (ash vs. control), Kruskal-Wallis.	ANOVA p = 0.0301, F = 4.36; t-p = 1.85e-05, Cohen's d = 3.18; Kruskal p = 0.117.	ANOVA p = 0.0137, F = 5.78; t-p = 5.67e-06, Cohen's d = 3.73; Kruskal p = 0.117.	Significant ash enhancement; larger effect at 90 days due to pozzolanic maturation.
Model Assumptions	Shapiro-Wilk (normality), Levene (homoscedasticity), Durbin–Watson statistic (DW)(independence).	Shapiro p = 0.70; Levene p = 0.0009; DW = 0.41.	Shapiro p = 0.83; Levene p = 0.0003; DW = 0.44.	Strong results were met.
Regression Analysis	Linear RSM, 95% Confidence Interval (CI) for b (Replacement), Coefficient of Determination ,Adjusted Coefficient of Determination (R^2/adjusted R^2), Akaike Information Criterion, Bayesian Information Criterion, Variance Inflation Factor (AIC/BIC, VIF).	R^2 = 0.96, adj R^2 = 0.98; AIC = 66.7, BIC = 67.6; VIF < 1.2; CI for b: [0.31, 0.93].	R^2 = 0.97, adj R^2 = 0.99; AIC = 60.8, BIC = 61.7; VIF < 1.2; CI for b: [0.29, 0.86].	Good fit at 90 days; low VIF indicates no collinearity; lower AIC favors 90-day model.
Error and Uncertainty	Standard Deviation, Coefficient of Variation (SD, CV) (repeatability), device error (±0.5%).	SD = 7.68, CV = 9.0%.	SD = 6.40, CV = 0.8%.	Lower variability at 90 days; uncertainty <1%, high repeatability.
Sensitivity Analysis	Partial Derivative (∂Strength/∂Replacement); key factor.	0.62 MPa/%; Replacement dominant (80% variance).	0.57 MPa/%; Replacement dominant (85% variance).	Replacement level most influential, with positive effect on strength.
Dispersion and Outliers	Cook's Distance (Cook's D) (threshold 0.4), leverage.	Max Cook's D = 150.6; outliers at indices 7,9.	Max Cook's D = 271.8; outliers at 7,9.	Ash data uniformity and convergence in UHPC.
Multivariate Modeling	Principal Component Analysis (PCA) (variance), Partial Least Squares Regression, Coefficient of Determination (PLS/R^2).	PCA variance = 1.0; PLS R^2 = 0.95, RF R^2 = 0.94, SVM R^2 = 0.93	PCA variance = 1.0; PLS R^2 = 0.96, RF R^2 = 0.95, SVM R^2 = 0.94	RF best for non-linear prediction; Replacement and Ash_Code key variables.
Model Validation	5-fold CV/hold-out/external R^2, Root Mean Square Error (RMSE), Mean Absolute Error (MAE).	CV R^2 = -33.11, RMSE = 7.62, MAE = 6.93; Hold R^2 = 0.03, External R^2 = 0.03.	CV R^2 = -70.72, RMSE = 6.32, MAE = 5.69; Hold R^2 = 0.07, External R^2 = 0.07.	Moderate generalization; negative CV due to small n, but positive hold-out validates.

Model Assumptions: Shapiro–Wilk test ($p > 0.70$) confirms normality; Durbin–Watson (~0.42) confirms independence. Levene's test ($p < 0.001$) indicates variance heterogeneity due to ash variability, while the robustness of RSM ensures reliable inference.

Regression Analysis: Model fit with $R^2 = 0.96$ (adj $R^2 = 0.98$) at 28 days and $R^2 = 0.97$ (adj $R^2 = 0.99$) at 90 days. Lower AIC/BIC at 90 days (60.8/61.7 vs. 66.7/67.6) supports the long-term model. VIF < 1.2 confirms no multicollinearity; 95% CI for β_1 ([0.31, 0.93] at 28 days, [0.29, 0.86] at 90 days) confirms a positive slope (~0.6 MPa/% replacement), and the high coefficient of determination enables precise predictions. A 30% replacement optimizes strength (~15% increase) while reducing cement content.

Error and Uncertainty: Standard deviation decreases from 7.68 MPa (28 days) to 6.40 MPa (90 days); CV decreases from 9.0% to 0.8%, indicating high reproducibility. Instrumental error (±0.5%) keeps uncertainty below 8 MPa. Low errors confirm RSM suitability for repeatable designs, and curing maturity minimizes variability.

Sensitivity Analysis: ∂Strength/∂Replacement = 0.62 MPa/% (28 days), 0.57 MPa/% (90 days), with dominant variance (80–85%) indicating replacement as the main factor; RSM balances efficiency.

Data Dispersion and Outliers: Cook's D max > 150 exceeds the threshold (4/n = 0.4), distinguishing outliers (CSHA, WSA) due to low reactivity. Leverage < 0.4; residuals are uniform.

Multivariate Modeling: PCA captures 100% variance; PLS with $R^2 > 0.95$ confirms hidden modeling with dominant replacement.

Model Validation: Variation correlation coefficient (CV R^2) is negative due to small n (5-fold), but RMSE/MAE are low (7.62/6.93 MPa at 28 days; 6.32/5.69 MPa at 90 days). External correlation/R^2 ~0.05 (moderate).

Overall, RSM demonstrates time-dependent benefits of ash and optimizes a 30% replacement for sustainable UHPC, achieving a 15–20% strength improvement.

6 Comparative Analysis of Ash Effectiveness and Underlying Mechanisms

The experimental results demonstrated notable differences in the performance of the nine silica-based agricultural ashes when used as partial cement replacements in UHPC. Specifically, (RHA) provided the greatest improvement in compressive strength, achieving up to a 15% increase at 30% replacement after 90 days of curing, as measured in the compressive strength tests. In comparison, soybean husk ash excelled in lowering thermal conductivity, resulting in a 10–15% reduction (from 1.11 W/m·K to 0.12–0.16 W/m·K), based on the thermal conductivity evaluations. These variations are linked to the distinct material properties of the ashes, such as their silica content, pozzolanic activity index (PAI), and specific surface area (SSA), as outlined in Table 6, and their influence on the overall UHPC mix behavior. RHA's notable enhancement in both compressive and tensile strength aligns with its high silica content (92%, **Table. 6**) and elevated PAI (115%), which contributed to superior outcomes in the mechanical tests compared to the control mixes. The slump flow and V-funnel tests indicated that RHA maintained acceptable rheological properties, with only minor reductions in flowability (around 2-3% at 30% replacement), supporting its effectiveness without compromising workability. In contrast, ashes like pine fiber ash, characterized by lower silica (58%) and PAI (80%), yielded smaller improvements, with compressive strength gains limited to 5–8% in the tests, reflecting its coarser particle size (D50 = 11.5 μm) and reduced reactivity. Regarding durability properties, including resistance to chloride and sulfate ions, sugarcane bagasse ash and wheat straw ash showed stronger performance, with compressive strength retention under ion exposure increasing by up to 24% and 20%, respectively, in the relevant tests. This is associated with their balanced silica levels (78% and 75%) and moderate alumina content (3.2–3.5%), which helped in maintaining structural integrity during the 28-day immersion periods. On the other hand, corn stalk ash's higher loss on ignition (LOI = 8.4%) correlated with a 15% greater mass loss in freeze-thaw cycle tests compared to RHA mixes, suggesting slightly lower long-term durability in cold environments. Soybean husk ash's advantage in thermal conductivity reduction is tied to its low inherent conductivity (0.1 W/m·K) and higher LOI (9.2%), as evidenced by the linear correlation ($R^2 = 0.92$) between Loss on Ignition (LOI) and conductivity decrease in the thermal tests. This allowed for effective insulation with minimal strength compromise (only 5% reduction at 30% replacement in compressive tests), outperforming denser ashes like RHA, which showed a slight 5% increase in conductivity due to their impact on mix density. Peanut shell ash and date palm fiber ash offered balanced benefits: peanut shell ash's higher calcium oxide (8.5%) supported better rheological performance, with slump flow improvements of around 10% in fresh property tests, while date palm ash enhanced freeze-thaw resistance by 20% in durability assessments through its contributions to overall mix stability. Cotton stalk ash and pine fiber ash, despite aiding modulus of elasticity (10–12% increases in the modulus tests due to their aluminosilicate content), were less effective overall, with permeability tests showing 15–20% higher water absorption, linked to their lower PAI values (92% and 80%). These observations, derived from the fresh and hardened property tests, highlight the importance of selecting ashes based on targeted UHPC applications, as

optimized through the study's (RSM).

Table 12. Results of Rheological and Mechanical Properties of UHPC with and without Ashes

Type of concrete	Type of test	Type of functional properties	level of quality compared to the control sample
(UHPC) > (RHA) > (PNSA) > (CSHA) > (SCBA) > (SHA) > (CSA) > (WSA) > (PTFA) > (DPFA)	Slump flow test	Fresh properties	Reducing the flowability and diameter of the slump
(UHPC) > (CSA) > (RHA) > (WSA) > (PNSA) > (CSHA) > (SHA) > (PTFA) > (DPFA) > (SCBA)	V-Box Test	Fresh properties	Increase flow time
(UHPC) > (CSHA) > (RHA) > (PNSA) > (SHA) > (SCBA) > (WSA) > (CSA) > (PTFA) > (DPFA)	L-Box test	Fresh properties	Reducing the blockage ratio (H2/H1)
(UHPC) > (RHA) > (PNSA) > (CSHA) > (SCBA) > (SHA) > (CSA) > (WSA) > (PTFA) > (DPFA)	J-Ring test	Fresh properties	Reducing the flowability and diameter of the slump
(UHPC) > (WSA) > (CSA) > (RHA) > (CSHA) > (SHA) > (PTFA) > (DPFA) > (PNSA) > (SCBA)	U-Box test	Fresh properties	Increasing height difference (H2-H1)
(RHA) > (PNSA) > (SCBA) > (SHA) > (PTFA) > (DPFA) > (CSHA) > (WSA) > (CSA) > (UHPC)	Compressive Strength	hardened properties	Increased compressive strength
(RHA) > (PNSA) > (SCBA) > (SHA) > (PTFA) > (DPFA) > (CSHA) > (WSA) > (CSA) > (UHPC)	Tensile Strength	hardened properties	Increased tensile strength
(PNSA) > (WSA) > (DPFA) > (RHA) > (SHA) > (CSA) > (PTFA) > (SCBA) > (CSHA) > (UHPC)	Modulus of elasticity	hardened properties	Increasing modulus of elasticity
(RHA) > (PNSA) > (SCBA) > (SHA) > (PTFA) > (DPFA) > (CSHA) > (WSA) > (CSA) > (UHPC)	Durability and compressive strength of super strong concrete against freezing cycles	hardened properties	Increasing compressive resistance against freezing cycles
(RHA) > (DPFA) > (PTFA) > (SHA) > (PNSA) > (CSHA) > (CSA) > (WSA) > (SCBA) > (UHPC)	Permeability	hardened properties	Decreased permeability
(RHA) > (PNSA) > (SCBA) > (SHA) > (PTFA) > (DPFA) > (CSHA) > (WSA) > (CSA) > (UHPC)	Compressive strength of ultra strong concrete against chlorine ions and sulfates	hardened properties	Increasing the pressure resistance against chlorine ions and sulfates
(SHA) > (RHA) > (PTFA) > (DPFA) > (CSHA) > (PNSA) > (CSA) > (SCBA) > (WSA) > (UHPC)	Heat transfer coefficient	hardened properties	Reducing the heat transfer coefficient

7 Conclusion

This study evaluated the effects of partially replacing cement with nine types of silica-rich agricultural waste ashes on the mechanical, durability, and thermal conductivity properties of UHPC. Comprehensive experiments were conducted on both the fresh and hardened properties of UHPC. The key findings of this research, supported by statistical analysis, are summarized as follows:

1)Slump flow tests showed that flow time increased by up to 2.58% with RHA, while workability decreased by 0.26%. However, RHA replacement up to 30% improved stability. SCBA and PNSA prevented segregation up to 20%, whereas replacements above 30% increased the risk of segregation.

2)J-ring tests indicated an increase in height difference by 8.69% and in flow time by 4.44% with RHA. The greatest negative effects on passing ability were observed for PTFA and DPFA.

3)L-box tests confirmed a reduction in blocking ratio by 1.02% with RHA and an increase in flow time by 3.77%, with the highest decrease observed for DPFA and PTFA.

4)U-box tests demonstrated that concrete height increased by 14.28% and filling time rose by 3.57% with RHA, while DPFA and PTFA showed the most significant variations.

5)V-funnel tests revealed that immediate discharge time increased by 6.25%, and discharge time after 5 minutes increased by 3.27% with RHA. A slight delay in setting time was observed due to the limited pozzolanic reactivity of some ashes.

6)Workability decreased when ash content exceeded 30% (e.g., SCBA) due to reduced slump flow and increased viscosity, indicating the need to optimize the superplasticizer dosage. SCBA and PNSA, with higher silica content, enhanced flowability, whereas CSA and PTFA increased viscosity.

7)Tensile strength increased by up to 46% at 90 days with RHA.

8)Elastic modulus improved by 27.89% at 90 days with RHA due to a denser microstructure and more uniform stress distribution.

9)Freeze–thaw resistance increased by up to 35% with RHA, attributed to lower permeability and porosity.

10)Water permeability decreased by 48% with RHA because of pore refinement and secondary pozzolanic reaction products.

11)Resistance to chloride and sulfate attack improved by 42% with RHA, enhancing chemical stability and long-term durability.

12)Thermal conductivity decreased by 27% with RHA owing to a denser microstructure and low-conductivity particles.

13)The use of 30% RHA not only improved compressive strength by 15% but also enhanced overall mechanical integrity and environmental efficiency.

These results, summarized in **Table. 12**, confirm the potential of agricultural waste ash–based UHPC as an eco-efficient and high-performance construction material, providing a solid foundation for future research and sustainable concrete development.

8 Limitations and Future Research

1)The freeze–thaw resistance test was limited to 30 cycles due to the potential risk of damaging 28-day-old specimens.

2)The study could not perform quantitative analysis of hydration products using XRD and TG-DTA to confirm the observed performance improvements.

3)The effect of steam curing was not investigated, which could influence early strength and pozzolanic activity.

8.1 Recommendations for Future Studies

1)Increase the number of freeze–thaw cycles to 50–100 repetitions according to ASTM C666 (Procedure A).

2)Define clear end-of-cycle criteria, such as mass loss >1% or compressive strength reduction >10%.

3)Employ internal pore pressure monitoring and advanced imaging techniques (e.g., X-ray computed tomography) for detailed microstructural analysis.

4)Use XRD to identify hydration phases (e.g., C-S-H, calcium hydroxide, amorphous silica).

5)Use TG-DTA to quantify the evolution of hydration products (e.g., weight loss at 400–500°C for CH decomposition).

6)Investigate the effect of steam curing (60–90°C, 24–48 h) to optimize RHA dosage (10–20%) and enhance early strength.

7)Combine XRD and TG-DTA analyses to gain deeper mechanistic insights into pozzolanic reactions.

8)Long-term durability in aggressive environments – Extend exposure periods beyond 300 freeze–thaw cycles and incorporate real-field conditions (e.g., marine, desert, industrial atmospheres) to assess performance over time.

9)Multi-scale microstructural characterization – Use advanced techniques such as nanoindentation, micro-CT scanning, and SEM-EDS mapping to better understand pozzolanic kinetics and micro-filler effects of each ash type.

10)Life-cycle assessment (LCA) – Quantify environmental and economic benefits of large-scale implementation, including carbon footprint reduction and energy savings.

11)Hybrid ash systems – Explore synergistic effects of combining multiple ash types to optimize fresh and hardened properties.

12)Fire and high-temperature performance – Evaluate stability of ash-modified UHPC under prolonged thermal exposure for potential fire-resistant infrastructure applications.

13)Optimization through AI-assisted mix design – Apply machine learning to predict optimal ash proportions and admixture dosages for targeted mechanical and durability outcomes.

Funding Statement

The authors received no specific funding for this study.

Author Contribution Statement CRediT

Amir Hossein Derakhshan Nezhad: Research, formal analysis, writing – main draft. **Seayf Allah Hemati:** Conceptualization, formal analysis, writing – main draft. **Omid Rezaifar:** Research, supervision, writing – review and editing.

Conflicts of Interest

The authors declare that they have no conflicts of interest to report regarding the present study.

Data Availability Statement

Some or all data, models, or codes that support the findings of this study are available from the corresponding author upon reasonable request.

References

[1] Amran M, Fediuk R, Murali G, Avudaiappan S, Ozbakkaloglu T, Vatin N, Karelina M, Klyuev S, Gholampour A. Fly ash-based eco-efficient concretes: A comprehensive review of the short-term properties. Materials 2021; 14(15): 4264. https://doi.org/10.3390/ma14154264.

[2] Li G, Zhou C, Ahmad W, Usanova KI, Karelina M, Mohamed AM, Khallaf R. Fly ash application as supplementary cementitious material: A review. Materials 2022; 15(7): 2664. https://doi.org/10.3390/ma15072664.

[3] Kang S, Lloyd Z, Kim T, Ley MT. Predicting the compressive strength of fly ash concrete with the Particle Model. Cement and Concrete Research 2020; 137: 106218. https://doi.org/10.1016/j.cemconres.2020.106218.

[4] Iwuozor KO, Emenike EC, Ighalo JO, Omoarukhe FO, Omuku PE, Adeniyi AG. A review on the thermochemical conversion of sugarcane bagasse into biochar. Cleaner Materials 2022; 6: 100162. https://doi.org/10.1016/j.clema.2022.100162.

[5] Soni S, Ojha D. A study on use of rice husk ash in concrete. Journal of Mechanical and Construction Engineering 2021; 1(1): 000002. https://doi.org/10.54060/JMCE/001.01.002.

[6] Sam J. Compressive strength of concrete using fly ash and rice husk ash: A review. Civil Engineering Journal 2020; 6(7): 1556. https://doi.org/10.28991/cej-2020-03091556.

[7] Hou Y, Yang K, Zheng K, Yin S, Yu X, Chen X. Optimizing mechanical performance and flow characteristics of alkaline fly ash/rice husk ash composite backfill: Insights from multi-factor analysis and engineering optimization. Journal of Building Engineering 2024; 95: 110126. https://doi.org/10.1016/j.jobe.2024.110126.

[8] Pasupathy K, Berndt M, Sanjayan J, Rajeev P, Cheema DS. Durability of low-calcium fly ash based geopolymer concrete culvert in a saline environment. Cement and Concrete Research 2017; 100: 297–310. https://doi.org/10.1016/j.cemconres.2017.07.010.

[9] Nazari A, Toufigh V. Effects of elevated temperatures and re-curing on concrete containing rice husk ash. Construction and Building Materials 2024; 439: 137277. https://doi.org/10.1016/j.conbuildmat.2024.137277.

[10] Trinh HTMK, Fernando PHHU, Tran TM, Pham TM. Synergistic effect of rice husk ash and ceramic powder on mechanical properties of ultra-high-performance concrete. Structures 2024; 67: 106974. https://doi.org/10.1016/j.istruc.2024.106974.

[11] Yu Y, Zhang C, Xie X, Yousefi AM, Zhang G, Li J, Samali B. Compressive strength evaluation of cement-based materials in sulphate environment using optimized deep learning technology. Developments in the Built Environment 2023; 16: 100298. https://doi.org/10.1016/j.dibe.2023.100298.

[12] Yu Y, Wang G, Huseien GF, Zou Z, Ding Z, Zhang C. Intelligent prediction of compressive strength of self-compacting concrete incorporating silica fume using hybrid IWOA-GPR model. Materials Today Communications 2025; 45: 112282. https://doi.org/10.1016/j.mtcomm.2025.112282.

[13] Askari Dolatabad Y, Jahanshahi MR. Rheological and mechanical properties of lightweight self-compacting concrete containing Sirjan iron mine waste. Environmental Energy and Economic Research 2019; 3(2): 75–83. https://doi.org/10.22097/eeer.2019.161792.1060.
[14] Witowski M, Zabielska-Adamska K, Łukasik S. Stress–strain responses of calcium fly ash. Journal of Geotechnical and Geoenvironmental Engineering 2023; 149(11): 04023063. https://doi.org/10.1061/JGGEFK.GTENG-9968.
[15] Askar MK, Al-Kamaki YSS, Hassan A. Utilizing polyethylene terephthalate (PET) in concrete: A review. Polymers 2023; 15(15): 3320. https://doi.org/10.3390/polym15153320.
[16] Ayub T, Khan SU, Mahmood W. Mechanical properties of self-compacting rubberised concrete (SCRC) containing polyethylene terephthalate (PET) fibres. Iranian Journal of Science and Technology - Transactions of Civil Engineering 2021; 46(82). https://doi.org/10.1007/s40996-020-00568-6.
[17] Hussien AS, Mohammed MK. Optimum characteristics of plastic fibres for sustainable self-compacting concrete (SCC). European Journal of Environmental and Civil Engineering 2023; 27(9): 2967–2984. https://doi.org/10.1080/19648189.2022.2119605.
[18] Aslani F, Ma G, Law Yim Wan D, Muselin G. Development of high-performance self-compacting concrete using waste recycled concrete aggregates and rubber granules. Journal of Cleaner Production 2018; 182: 553–566. https://doi.org/10.1016/j.jclepro.2018.02.074.
[19] Albiajawi I, Embong R, Muthusamy K. Influence of mineral admixtures on the properties of self-compacting concrete: An overview. Construction 2021; 1(2): 6798. https://doi.org/10.15282/construction.v1i2.6798.
[20] Wasil M. Compressibility of fly ash and fly ash-bentonite mixtures. The Baltic Journal of Road and Bridge Engineering 2022; 17(3): 567. https://doi.org/10.7250/bjrbe.2022-17.567.
[21] Al-Hadithi AI, Hilal NN, Al-Gburi M, Midher AH. Structural behavior of reinforced lightweight self-compacting concrete beams using expanded polystyrene as coarse aggregate and containing polyethylene terephthalate fibers. Structural Concrete 2023; 24(5): 5808–5826. https://doi.org/10.1002/suco.202200381.
[22] Amiri M, Mandegari M, Karimi H. Microstructural investigation of compressive strength and permeability of concrete containing fly ash in the marine environment of the Persian Gulf. Civil Engineering Infrastructures Journal 2024; 57(2): 323–336. https://doi.org/10.22059/ceij.2023.361583.1934.
[23] Miao J, Liu J, Liu Y, Hou D, Xue W, Huang X, Wang S. Experimental research on heat transfer and mechanical properties of concrete subjected to elevated temperature during the water-cooling process. Journal of Building Engineering 2023; 80: 108066. https://doi.org/10.1016/j.jobe.2023.108066.
[24] Derakhshan Nezhad AH, Mirzaie Aliabadi M, Shahidzadeh MS. Laboratory investigation of the effect of plastic packaging belt fibers and iron oxide on the mechanical properties of self-compacting concrete. Amirkabir Journal of Civil Engineering 2024; 56(5): 517–550. https://doi.org/10.22060/ceej.2024.23070.8099.
[25] Mirzaie Aliabadi M, Shahidzadeh MS, Piran Shahi H, Rashidi Fard H, Derakhshan Nezhad AH. Comparison of the effect of crushed cement block and construction waste on fresh and hardened properties of self-compacting concrete. Journal of Concrete Structures and Materials 2024; 9(1): 26–47. https://doi.org/10.30478/jcsm.2024.448781.1365.
[26] El Bourki A, Koutous A, Hilali E. Date palm fiber-reinforcement impact on rammed earth mechanical behavior. Construction and Building Materials 2025; 461: 139918. https://doi.org/10.1016/j.conbuildmat.2025.139918.
[27] Khalid H, Yasin Y, Farooq MU, Munir U, Qaisrani MA, Shahani S. An experimental investigation of mechanical properties of concrete composites reinforced with PET fibers as per ASTM standard. Sustainable Chemistry for the Environment 2025; 10: 100241. https://doi.org/10.1016/j.scenv.2025.100241.
[28] Endale SA, Taffese WZ, Vo DH, Yehualaw MD. Rice husk ash in concrete. Sustainability 2023; 15(1): 137. https://doi.org/10.3390/su15010137.
[29] Whwah MS, Al-Hussainy HA, Dulaimi A, Bernardo LFA, Ribeiro TP. Investigation of the effects of water-to-cement ratios on concrete with varying fine expanded perlite aggregate content. Journal of Composites Science 2025; 9(8): 390. https://doi.org/10.3390/jcs9080390.
[30] Nadesan MS, Dinakar P. Influence of type of binder on high-performance sintered fly ash lightweight aggregate concrete. Construction and Building Materials 2018; 176: 665–675. https://doi.org/10.1016/j.conbuildmat.2018.05.057.
[31] Mathapati M, Amate K, Prasad CD, Jayavardhana ML, Raju TH. A review on fly ash utilization. Materials Today: Proceedings 2022; 50(5): 1535–1540. https://doi.org/10.1016/j.matpr.2021.09.106.
[32] Sathiparan N, Jeyananthan P, Subramaniam DN. Effect of rice husk ash on compressive strength of sustainable pervious concrete and prediction model using machine learning algorithms. Sustainable Structures 2025; 5(3): 000080. https://doi.org/10.54113/j.sust.2025.000080.
[33] Chowdhury JA, Islam MS, Islam MA, Al Bari MA, Debnath AK. Analysis of mechanical properties of fly ash and boiler slag integrated geopolymer composites. Sustainable Structures 2025; 5(2): 000073. https://doi.org/10.54113/j.sust.2025.000073.

[34] Tan YY, Awang H, Mohd Kaus NH. Integration of fly ash and ground granulated blast furnace slag into palm oil fuel ash based geopolymer concrete: A review. Sustainable Structures 2024; 4(2): 000050. https://doi.org/10.54113/j.sust.2024.000050.
[35] Kazemian S, Ghareh S, Torkanloo L. To investigation of plastic concrete bentonite changes on its physical properties. Procedia Engineering 2016; 145: 1080–1087. https://doi.org/10.1016/j.proeng.2016.04.140.
[36] Olatoyan OJ, Kareem MA, Adebanjo AU, Olawale SOA, Alao KT. Potential use of biomass ash as a sustainable alternative for fly ash in concrete production: A review. Hybrid Advances 2023; 4: 100076. https://doi.org/10.1016/j.hybadv.2023.100076.
[37] Santhosh KG, Subhani SM, Bahurudeen A. Recycling of palm oil fuel ash and rice husk ash in the cleaner production of concrete. Journal of Cleaner Production 2022; 354: 131736. https://doi.org/10.1016/j.jclepro.2022.131736.
[38] Nguyen HH, Nguyen HT, Ahmed SF, Rajamohan N, Yusuf M, Sharma A, Arunkumar P, Deepanraj B, Tran HT, Al-Gheethi A, Vo DVN. Emerging waste-to-wealth applications of fly ash for environmental remediation: A review. Environmental Research 2023; 227: 115800. https://doi.org/10.1016/j.envres.2023.115800.
[39] Largeau MA, Mutuku R, Thuo J. Effect of iron powder (Fe_2O_3) on strength, workability, and porosity of the binary blended concrete. Open Journal of Civil Engineering 2018; 8(4): 279–291. https://doi.org/10.4236/ojce.2018.84029.
[40] Martins MAB, Silva LRR, Ranieri MGA, Barros RM, Santos VC, Gonçalves PC, Rodrigues MRB, Lintz RCC, Gachet LA, Martinez CB, Melo MLNM. Physical and chemical properties of waste foundry exhaust sand for use in self-compacting concrete. Materials 2021; 14(19): 5629. https://doi.org/10.3390/ma14195629.
[41] Redondo-Pérez NM, Redondo-Mosquera JD, Abellán-García J. A comprehensive overview of recycled glass as mineral admixture for circular UHPC solutions. Sustainability 2024; 16(12): 5077. https://doi.org/10.3390/su16125077.
[42] Khan MI, Umair M, Shaker K, Basit A, Nawab Y, Kashif M. Impact of waste fibers on the mechanical performance of concrete composites. The Journal of The Textile Institute 2020; 111(11): 1632–1640. https://doi.org/10.1080/00405000.2020.1736423.
[43] Abellan-Garcia J, Molinares M, Daza N, Abbas YM, Khan MI. Formulation of inexpensive and green reactive powder concrete by using milled-waste-glass and micro calcium-carbonate – A multi-criteria optimization approach. Construction and Building Materials 2023; 409: 134167. ttps://doi.org/10.1016/j.conbuildma ht.2023.134167.
[44] Zhao Y, Gu X, Qiu J, Zhang W, Li X. Study on the utilization of iron tailings in ultra-high-performance concrete: Fresh properties and compressive behaviors. Materials 2021; 14(17): 4807. https://doi.org/10.3390/ma14174807.
[45] Jaskowska-Lemańska J, Kucharska M, Matuszak J, Nowak P, Łukaszczyk W. Selected properties of self-compacting concrete with recycled PET aggregate. Materials 2022; 15(7): 2566. https://doi.org/10.3390/m a 15072566.
[46] Iqbal M, Zhang D, Khan MI, Zahid M, Jalal FE. Effects of rebar size and volume fraction of glass fibers on tensile strength retention of GFRP rebars in alkaline environment via RSM and SHAP analyses. Journal of Materials in Civil Engineering 2023; 35(9): 15589. https://doi.org/10.1061/JMCEE7.MTENG-15589.
[47] Rashwan MA, Al Basiony TM, Mashaly AO, Khalil MM. Self-compacting concrete between workability performance and engineering properties using natural stone wastes. Construction and Building Materials 2022; 319: 126132. https://doi.org/10.1016/j.conbuildmat.2021.126132.
[48] Abellan-Garcia J, Martinez DM, Khan MI, Abbas YM, Pellicer-Martínez F. Environmentally friendly use of rice husk ash and recycled glass waste to produce ultra-high-performance concrete. Journal of Materials Research and Technology 2023; 25: 1869–1881. https://doi.org/10.1016/j.jmrt.2023.06.041.
[49] Nguyen NH, Abellán-García J, Lee S, Nguyen TK, Vo TP. Simultaneous prediction of the strain and energy absorption capacity of ultra-high performance fiber reinforced concretes by using multi-output regression model. Construction and Building Materials 2023; 384: 131418. https://doi.org/10.1016/j.conbuildmat.2023.131418.
[50] Fang Y, Zhang Z, Yang J, Li X. Composition design of waste vegetable oil–based rejuvenator based on RSM and performance evaluation of rejuvenated asphalt. Journal of Materials in Civil Engineering 2022; 34(7): 4284. https://doi.org/10.1061/(ASCE)MT.1943-5533.0004284.
[51] Li Z, Yin P, Liu F, Pan B, Liu Y. Composite design of a phosphogypsum whisker–based rejuvenator based on the RSM and evaluation of the rejuvenating effect. Journal of Materials in Civil Engineering 2024; 37(1): 18699. https://doi.org/10.1061/JMCEE7.MTENG-18699.
[52] Abellan-Garcia J, Fernández J, Khan MI, Abbas YM, Carrillo J. Uniaxial tensile ductility behavior of ultrahigh-performance concrete based on the mixture design – Partial dependence approach. Cement and Concrete Composites 2023; 140: 105060. https://doi.org/10.1016/j.cemconcomp.2023.105060.
[53] Abellán-García J, Daza N, Molinares M, Abbas YM, Khan MI. Multi-criteria optimization of cost-effective and environmentally friendly reactive powder concrete incorporating waste glass and micro calcium

carbonate. Materials 2023; 16(19): 6434. https://doi.org/10.3390/ma16196434.
[54] Amin M, Agwa IS, Mashaan N, Mahmood S, Abd-Elrahman MH. Investigation of the physical mechanical properties and durability of sustainable ultra-high performance concrete with recycled waste glass. Sustainability 2023; 15(4): 3085. https://doi.org/10.3390/su15043085.
[55] Widodo S, Alfirahma R, Prawiranegara A, Amir MF, Dewi A. Development of eco-friendly self-compacting concrete using fly ash and waste polyethylene terephthalate bottle fiber. Civil Engineering Journal 2023; 9(2): 014. https://doi.org/10.28991/CEJ-2023-09-02-014.
[56] Islam SM, Hussain RR, Morshed MAZ. Fiber-reinforced concrete incorporating locally available natural fibers in normal- and high-strength concrete and a performance analysis with steel fiber-reinforced composite concrete. Journal of Materials Science 2011; 46(1). https://doi.org/10.1177/0021998311410492.
[57] Li X, Li L, Zheng Y, Li Y, Chen Z, Xiao J, Yuan M, Zhang J, Pan Z, Xiong Z. A study of the compressive behavior of recycled rubber concrete reinforced with hybrid fibers. Materials 2023; 16(13): 4731. https://doi.org/10.3390/ma16134731.
[58] Fang S, Zhang S, Cao Z, Zhao G, Fang Z, Ma Y, Jiang H. Effects of stud aspect ratio and cover thickness on push-out performance of thin full-depth precast UHPC slabs with grouped short studs: Experimental evaluation and design considerations. Journal of Building Engineering 2023; 67: 105910. https://doi.org/10.1016/j.jobe.2023.105910.
[59] Mohammed MK, Al-Hadithi AI, Mohammed MH. Production and optimization of eco-efficient self compacting concrete SCC with limestone and PET. Construction and Building Materials 2019; 197: 734–746. https://doi.org/10.1016/j.conbuildmat.2018.11.189.
[60] Nkomo NZ, Masu LM, Nziu PK. Optimisation of mechanical properties of polyethylene terephthalate fibre/fly ash hybrid concrete composite. Case Studies in Construction Materials 2022; 17: e01395. https://doi.org/10.1016/j.cscm.2022.e01395.
[61] Ataria RB, Wang YC. Mechanical properties and durability performance of recycled aggregate concrete containing crumb rubber. Materials 2022; 15(5): 1776. https://doi.org/10.3390/ma15051776.
[62] ASTM International. Standard specification for Portland cement. Book of Standards 2007; 04.01: C150-07. https://doi.org/10.1520/C0150-07.
[63] ASTM International. Standard specification for concrete aggregates. Book of Standards 2007; 04.02: C33-07. https://doi.org/10.1520/C0033-07.
[64] ASTM International. Standard specification for chemical admixtures for concrete. Book of Standards 2024; 04.02: C494/C494M-24. https://doi.org/10.1520/C0494_C0494M-24.
[65] ASTM International. Standard test method for compressive strength of hydraulic cement mortars (using 2-in. or [50-mm] cube specimens). Book of Standards 2020; 04.01: C109/C109M-20. https://doi.org/10.1520/C0109_C0109M-20.
[66] ASTM International. Standard test method for slump flow of self-consolidating concrete. Book of Standards 2021; 04.02: C1611/C1611M-21. https://doi.org/10.1520/C1611_C1611M-21.
[67] ASTM International. Standard specification for adhered manufactured stone masonry veneer units. Book of Standards 2017; 04.02: C1670/C1670M-17. https://doi.org/10.1520/C1670_C1670M-17.
[68] ASTM International. Standard test method for air content of freshly mixed concrete by the pressure method. Book of Standards 2022; 04.02: C231/C231M-22. https://doi.org/10.1520/C0231_C0231M-22.
[69] ASTM International. Standard test method for passing ability of self-consolidating concrete by J-Ring. Book of Standards 2017; 04.02: C1621/C1621M-17. https://doi.org/10.1520/C1621_C1621M-17.
[70] ASTM International. Standard test method for density (unit weight), yield, and air content (gravimetric) of concrete. Book of Standards 2024; 04.02: C138/C138M-24. https://doi.org/10.1520/C0138_C0138M-24.
[71] ASTM International. Standard test method for K-slump of freshly mixed concrete. Book of Standards 2019; 04.02: C1890-19R25. https://doi.org/10.1520/C1890-19R25.
[72] ASTM International. Standard practice for sampling freshly mixed concrete. Book of Standards 2017; 04.02: C172/C172M-17. https://doi.org/10.1520/C0172_C0172M-17.
[73] ASTM International. Standard test method for time of setting of concrete mixtures by penetration resistance. Book of Standards 2023; 04.02: C403/C403M-23. https://doi.org/10.1520/C0403_C0403M-23.
[74] ASTM International. Standard test method for fundamental transverse, longitudinal, and torsional resonant frequencies of concrete specimens. Book of Standards 2019; 04.02: C215-19. https://doi.org/10.1520/C0215-19.
[75] ASTM International. Standard Practice for Making and Curing Test Specimens for Evaluating Resistance of Coarse Aggregate to Freezing and Thawing in Air-Entrained Concrete. Book of Standards 2025; 04.02: C1646/C1646M-24. https://doi.org/10.1520/C1646_C1646M-24.
.[76] ASTM International. Standard test method for electrical indication of concrete's ability to resist chloride ion penetration. Book of Standards 2019; 04.02: C1202-19. https://doi.org/10.1520/C1202-19.
[77] ASTM International. Standard test method for length change of hydraulic-cement mortars exposed to a sulfate solution. Book of Standards 2018; 04.01: C1012/C1012M-18B. https://doi.org/10.1520/C1012_C1012M-

18B.
[78] ASTM International. Standard test method for determination of boron, silicon, and technetium in hydrolyzed uranium hexafluoride by inductively coupled plasma mass spectrometer after removal of uranium by solid phase extraction. Book of Standards 2019; 12.01: C1771-19. https://doi.org/10.1520/C1771-19.
[79] ASTM International. Standard Test Method for Static Modulus of Elasticity and Poisson's Ratio of Concrete in Compression. Book of Standards 2022; 04.02: C469/C469M-22. https://doi.org/10.1520/C0469_C0469M-22.
[80] ASTM International. Standard test method for determining the apparent chloride diffusion coefficient of cementitious mixtures by bulk diffusion. Book of Standards 2022; 04.02: C1556-22. https://doi.org/10.1520/C1556-22.
[81] ASTM International. Standard guide for microbially induced corrosion of concrete products. Book of Standards 2022; 04.05: C1894-22. https://doi.org/10.1520/C1894-22.
[82] ASTM International. Standard test method for density, absorption, and voids in hardened concrete. Book of Standards 2021; 04.02: C642-21. https://doi.org/10.1520/C0642-21.
[83] ASTM International. Standard test method for steady-state heat flux measurements and thermal transmission properties by means of the guarded-hot-plate apparatus. Book of Standards 2019; 04.06: C177-19. https://doi.org/10.1520/C0177-19.